

# Full range spectral correlations and their spectral form factors in chaotic and integrable models

Ruth Shir,<sup>\*</sup> Pablo Martinez-Azcona,<sup>\*</sup> and Aurélie Chenu<sup>†</sup>

*Department of Physics and Materials Science, University of Luxembourg, L-1511 Luxembourg, Luxembourg*

(Dated: April 19, 2024)

Correlations between the eigenenergies of a system's spectrum can be a defining feature of quantum chaos. We characterize correlations between energies for all spectral distances by studying the distributions of  $k$ -th neighbor level spacings ( $knLS$ ) and compute their associated  $k$ -th neighbor spectral form factor ( $knSFF$ ). Specifically, we find analytical expressions for these signatures in paradigmatic models of quantum chaos, namely the three Gaussian ensembles of random matrix theory, and in integrable models, taken as systems with completely uncorrelated spectra (the Poissonian ensemble). The spectral distance decomposition of the SFF allows us to probe the contribution of each individual  $knLS$  to the ramp. The latter is a characteristic feature of quantum chaos, and we show how each spectral distance participates in building it—the linear ramp cannot be formed by short-range energy correlations only. We illustrate our findings in the XXZ spin chain with disorder, which interpolates between chaotic and integrable behavior.

Quantum many-body systems are studied in fields as diverse as condensed matter, statistical mechanics, quantum information, and high-energy physics. Although their spectra are usually too complicated to be described and studied analytically, certain statistical properties are universally shared among different systems. These spectral statistical properties have become a probe of whether a quantum system is chaotic or integrable. Specifically, the statistics of spectral spacings is one such probe of the underlying nature of a system. In a quantum chaotic system, it evidences that the eigenenergies are not independently distributed but rather correlated in such a way that no two values can lie too close together. By contrast, the spectral spacings of quantum integrable systems exhibit no such correlations—a property that can be attributed to the existence of an extensive number conserved charges in such systems [1].

The distributions of nearest-neighbor level spacings are closely related to the statistics of certain random matrices: those of quantum chaotic systems are close to Gaussian random ensembles, while those of generic integrable systems follow the statistics of a diagonal matrix with (real) random entries. Hence, the study of random matrices has become central to the study of complex chaotic and integrable quantum systems. The relation between random matrices and quantum chaos is described in e.g. [2, 3], with some of the foundational works related in e.g. [4–11].

Importantly, the analogy between complex quantum systems and random matrices does not stop at the level of nearest-neighbor spacing distribution. The existence (or not) of spectral correlations extends beyond nearest-neighbor level spacings and can be probed by other measures, including the spectral rigidity, the number variance, and the spectral form factor (SFF) [3, 12]. These

quantities can be computed analytically with random matrix theory [2]. The statistical spectral properties of complex quantum systems follow the random matrix predictions pretty well, with deviations occurring mainly at long-range spectral distances.

A large part of this work focuses on the spectral form factor, which is a dynamical signature of quantum chaos. The SFF is the Fourier transform of the two-point eigenvalue correlation function of a matrix. As such, it includes all spectral distances. It is related to physical time-dependent observables such as operator autocorrelation functions, the survival probability of quantum states, or the analytical continuation of the partition function. It has been used to study spectral properties of quantum systems ranging from nuclear physics and physical chemistry, all the way to black holes, see e.g. [13–21]. As a time-dependent function, the behavior of the SFF at different time scales depends on the underlying spectrum. For complex systems (whose energies are usually not related to each other in any special way, i.e. they are incommensurate), a single set of eigenvalues results in a very noisy time-dependent function [22], such that some kind of averaging is required to see its key features. After such averaging, the SFF can be used to distinguish between chaotic and integrable spectra. In both kinds of systems, it starts with an initial decay at early times and, for systems of finite size, stabilizes at a ‘plateau’ at late times (times proportional to the inverse of the average level spacing). The behavior in-between depends on whether the spectrum is chaotic—in which case the SFF first goes below the plateau value before joining it up via a linear ‘ramp’, forming a ‘correlation hole’—or integrable—the SFF then goes almost directly from the decay to the plateau without any hole. Since the SFF involves all energy differences, it probes all ranges of correlations (with equal weight at infinite temperature) in a system's spectrum.

Our results, based on the  $k$ th neighbor spectral distributions in random matrices, show how each spectral distance contributes to the SFF. Specifically, we derive the

---

<sup>\*</sup> These authors contributed equally to the work

<sup>†</sup> [aurelia.chenu@uni.lu](mailto:aurelia.chenu@uni.lu)

$k$ th neighbor level spacing distributions ( $knLS$ ). Their Fourier transforms allow us to introduce the  $k$ th neighbor spectral form factors ( $knSFF$ ) and thus perform a *spectral distance decomposition of the SFF*. We then show how the latter builds up, with time, from contributions of correlations between eigenenergies further apart.

We provide analytical results for the three Gaussian ensembles, namely the Orthogonal (GOE), Unitary (GUE), and Symplectic (GSE) ensembles, whose spectral statistics is representative of that in quantum chaotic systems—the ensemble depending on the properties of their Hamiltonian under time reversal. We also provide results for the ‘Poissonian’ ensemble, constructed from diagonal matrices with random entries taken from a uniform distribution, and whose statistics are representative of the spectral statistics of quantum integrable systems. Our analytical results are based on tractable approximations, that we detail and verify. As such, a first result of this work is to derive the probability of the  $knLS$  based on Wigner’s original approach, that is, considering the joint probability density of eigenvalues of the largest possible matrix with a  $k$ -th spacing. The variance of this distribution can help identify when a physical model deviates from the idealized chaotic or integrable models. Knowledge of those distributions allows us to analytically find the contribution of each level distance to the SFF ( $knSFF$ ). Specifically, we show how the  $knSFF$  can be written as a Gaussian envelope and an oscillating function, part of the latter capturing the non-Gaussianity of the  $knLS$  distributions. We show how this specific form is important to build the linear ramp, and how correlations between eigenvalues further apart participate in building the linear ramp. Such decomposition also allows us to introduce refined dynamical signature of chaos. Indeed, we find that the minimum value of the  $knSFF$  behaves very differently for the Gaussian ensembles than for the Poissonian case.

The tools and analytical results we introduce can be used to see when and how a complex many-body quantum system deviates from the ideal (chaotic or integrable) cases mentioned above. We illustrate our methodology by examining a physical system, namely, an XXZ spin chain with disorder, a model which is often used in the context of many-body localization (see e.g. [23–28]) and whose SFF has been studied [28–31]. This system shows a transition from chaos to integrability as a function of the disorder’s strength.

The paper is structured as follows: Section I briefly introduces the models we consider. Section II presents a summary of our main results. The derivations and implications are detailed in the rest of the paper. In Sec. III we study spectral statistics, first providing an approximated derivation of the  $knLS$  distributions. We show how the variance of the  $knLS$  distribution can be used to diagnose quantum chaos, and discuss its results in the XXZ spin chain with disorder. In Section IV we study dynamical signatures of chaos. In particular, we introduce a decomposition of the SFF in terms of the above-

mentioned  $k$ th neighbor level spacings. We introduce a toy model whose spectrum has mixed features of spectral correlations, namely, only nearest-neighbor correlations according to the Wigner distributions of level spacings, and verify that its SFF does not exhibit a linear ramp. Section V details a dissipative protocol to measure correlation functions related to the  $knSFF$ . Finally, Section VI provides conclusions and a discussion of our results as well as future directions in the light of this work.

## I. THE MODELS

In this work, we consider Hermitian Hamiltonians, each with a finite discrete spectrum (or energy window) with  $N$  eigenvalues,  $\{E_1, E_2, \dots, E_N\}$ , that we arrange in increasing order. We define the set of  $k$ th nearest-neighbor level spacings ( $knLS$ ) for  $1 \leq k \leq N - 1$  as  $\{s_1^{(k)}, s_2^{(k)}, \dots, s_{N-k}^{(k)}\}$ , where  $s_i^{(k)} = E_{i+k} - E_i$  for  $1 \leq i \leq N - k$  integer. For example,  $k = 1$  gives the usual set of nearest-neighbor spacings. We always unfold the spectrum so that the average distance between eigenvalues is equal to one,  $\langle s^{(1)} \rangle = 1$ . Thus, it is expected that  $\langle s^{(k)} \rangle = k$ .

### A. Gaussian and Poissonian ensembles

A Gaussian random matrix can be described by the joint probability density of its  $N$  eigenvalues, which reads [2]

$$\rho_\beta(E_1, \dots, E_N) = C \prod_{1 \leq i < j \leq N} |E_i - E_j|^\beta e^{-A \sum_{i=1}^N E_i^2}, \quad (1)$$

where  $\beta$  is the Dyson index distinguishing the different ensembles, namely  $\beta = 1, 2, 4$  for the GOE, GUE, GSE, respectively. The constant  $C$  will not play a role in this work and  $A$  sets the energy scale, which we keep free for now. A random matrix taken from a Gaussian ensemble is constructed by sampling each matrix element from Gaussian distributions, as we detail in Appendix A for completeness.

A random matrix taken from the Poissonian ensemble is a diagonal matrix with elements sampled from a uniform distribution. We label this ensemble with  $\beta = 0$  for convenience.

### B. The XXZ spin chain with disorder

The tools and methodology we introduce in this work are illustrated in a physical model. Specifically, we quantify how closely a many-body quantum system follows the Gaussian or Poissonian random matrix ensembles. We choose the XXZ spin chain with a varying amount of disorder in on-site magnetic field,  $\hat{H} = \hat{H}_{\text{XXZ}} + \hat{H}_{\text{dis}}$ , because

this model is known to interpolate between chaos and integrability as a function of disorder strength. The Heisenberg XXZ spin-chain Hamiltonian for  $L$  spins reads

$$\hat{H}_{\text{XXZ}} = \sum_{n=1}^L (\hat{S}_n^x \hat{S}_{n+1}^x + \hat{S}_n^y \hat{S}_{n+1}^y + J_z \hat{S}_n^z \hat{S}_{n+1}^z), \quad (2)$$

where  $\hat{S}_n^{x,y,z}$  are spin 1/2 operators on site  $n$ . We assume periodic boundary conditions. This model is known to be integrable and can be solved using the Bethe ansatz [32]. Adding on-site magnetic fields with random strengths

$$\hat{H}_{\text{dis}} = \sum_{n=1}^L h_n^z \hat{S}_n^z, \quad (3)$$

where  $h_n^z$  are real random numbers taken from a uniform distribution  $\mathcal{U}_{[-W/2, W/2]}$ , changes the integrability properties of the XXZ chain as a function of the disorder strength  $W$ . Roughly speaking, when  $W$  is small (but not too small), integrability is broken, while as  $W$  increases, integrability is restored. In the chaotic regime, the spectral statistics agree with those of GOE due to the system's time-reversal symmetry [33]. The XXZ Hamiltonian with the disorder term (3) conserves the total spin in the  $z$ -direction; in other words, it commutes with the operator  $\hat{S}^z = \sum_{n=1}^L \hat{S}_n^z$ . The Hamiltonian thus does not mix sectors of different  $\hat{S}^z$  eigenvalues, and we can work in one such sector. We choose to work in the sector with half of the spins up and half of the spins down, which is of dimension  $\binom{L}{L/2}$ . We present results for  $L = 16$  for which the Hilbert space dimension in the above-mentioned sector is 12,870. In practice, however, we draw our statistics from  $N = 200$  eigenvalues around the densest part of the spectrum.

## II. SUMMARY OF MAIN RESULTS

This section provides an overview of our main results, whose derivation is given in later sections, along with further details.

### A. Beyond Wigner's surmise

For the Gaussian random matrix ensembles, the nearest neighbor level-spacing (nnLS) distribution ( $k = 1$ ) follows the Wigner surmise,  $\mathcal{P}_\beta(s) = C_\beta s^\beta e^{-A_\beta s^2}$ , where  $\beta$  is a parameter that distinguishes between the three Gaussian ensembles, GOE ( $\beta = 1$ ), GUE ( $\beta = 2$ ) and GSE ( $\beta = 4$ ). We first derive the probability distribution for any energy spacing  $s^{(k)}$  [34–39] by characterizing its variance, which can probe spectral correlations.

As mentioned above, the average of the distribution of  $s^{(k)}$  for an unfolded spectrum is  $k$ . We show in Section III that for the three Gaussian ensembles the  $k$ th neighbor

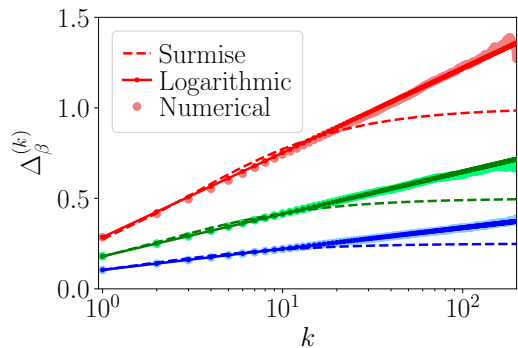


FIG. 1. **Variance of the distributions**  $\mathcal{P}_\beta^{(k)}(s)$  as a function of spectral distance  $k$  for the different Gaussian ensembles: GOE (red), GUE (green) and GSE (blue). We compare numerical results (circles) with analytical results from the surmise (4) and from the logarithmic behavior (6). Results are sampled from random matrices of dimension 1000, from which we sampled the  $N = 200$  central eigenvalues and we average over  $N_{\text{av}} = 1000$  realizations of the ensembles.

level-spacing ( $k$ nLS) distribution is approximately given by

$$\mathcal{P}_\beta^{(k)}(s) \approx C_\alpha s^\alpha e^{-A_\alpha s^2}, \quad (4)$$

where  $\alpha$  depends on the spectral distance  $k$  and the ensemble index  $\beta$  through

$$\alpha = \frac{k(k+1)}{2}\beta + k - 1. \quad (5)$$

The values of  $A_\alpha$  and  $C_\alpha$  are detailed in Eqs. (25a) and (25b), respectively.

The average of this distribution  $\mathcal{P}_\beta^{(k)}(s)$  is  $\langle s \rangle = k$ , and its variance is  $\Delta_\beta^{(k)} \equiv \langle s^2 \rangle - \langle s \rangle^2 = \left( \frac{\alpha+1}{2A_\alpha} \right) - k^2$ , which saturates to  $1/\beta$  for large  $k$ . In fact, this variance of the generalized surmise (4) does not appropriately capture the behavior of the exact distribution at large  $k$ . Instead, it follows

$$\Delta_\beta^{(k)} = \frac{2}{\pi^2\beta} \ln k + \text{const}. \quad (6)$$

Interestingly, this result behaves as the number-variance,  $\Sigma^2(L)$  at  $L = k$ , for the Gaussian ensembles, apart from the constant value and the fact that  $k$  is discrete here. In [40] it was observed that  $\Sigma_\beta^2(k) = \Delta_\beta^{(k)} + 1/6$ , from which the constant can be read off as  $\frac{2}{\pi^2} [\ln 2\pi + \gamma + 1 - \pi^2/8] - 1/6$  for GOE,  $\frac{1}{\pi^2} [\ln 2\pi + \gamma + 1] - 1/6$  for GUE and  $\frac{1}{2\pi^2} [\ln 4\pi + \gamma + 1 + \pi^2/8] - 1/6$  for GSE, where  $\gamma \approx 0.57721$  is Euler's constant. Figure 1 illustrates the different results for the variance of the  $k$ th level distribution for the three random matrix ensembles [41].

For the Poissonian ensemble (which we will label with  $\beta = 0$ ), the  $k$ th neighbor spacing distribution reads

$$\mathcal{P}_0^{(k)}(s) = \frac{1}{(k-1)!} s^{k-1} e^{-s}, \quad (7)$$

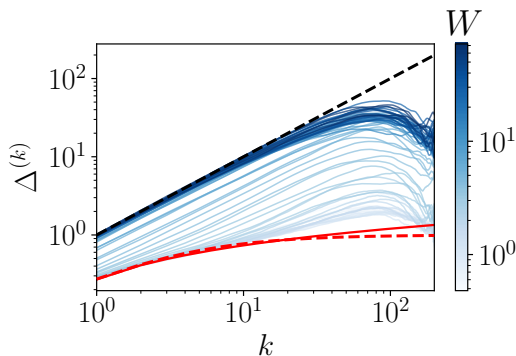


FIG. 2. **Variance of the  $knLS$  distribution as a function of the neighbor degree  $k$  for the XXZ model** (solid blue lines), GOE (red lines, dashed for the surmise, plain for the log) and Poisson (dashed black line). The color scale shows different disorder strengths  $W$ .

with variance given precisely by

$$\Delta_0^{(k)} = k, \quad (8)$$

which is exactly the result for the number variance,  $\Sigma^2(L)$ , of the Poissonian ensemble at integer  $L = k$ .

So the variance of the Poissonian ensemble increases linearly with  $k$ , which contrasts with the logarithmic scaling in the Gaussian ensembles. This can be understood because the energies in the Poisson ensemble are completely uncorrelated—thus unconstrained to spread—while the correlations in the Gaussian ensembles restrict the width of the spacing distributions for longer ranges  $k$ . The variance thus witnesses the strength of energy correlations, and can be used to distinguish systems with integrable or chaotic spectral statistics. This can be useful to identify when a many-body system starts deviating from the Gaussian random matrices and Poissonian results, as Fig. 2 illustrates for the disordered XXZ chain.

### B. Spectral-distance decomposition of the SFF

After having found the structure of level spacing distributions beyond nearest neighbors, we ask how each set of level spacings contributes to the spectral form factor. As may be expected, nearest-neighbor correlations are not enough to determine its full time-dependent profile and longer-range spectral correlations are needed as time increases. The SFF is the simplest nontrivial measure of spectral correlations and indistinguishably accounts for all energy neighbors. We will take its simplest definition, at infinite temperature, as  $S_t = \langle \sum_{m,n}^N e^{-i(E_n - E_m)t} / N^2 \rangle$ , where the angle brackets denote an ensemble average. We are interested in characterizing the contribution of each  $knLS$  to the SFF, and in a similar spirit to Wilkie and Brumer [14], we define

the  $k$ th neighbor SFF ( $knSFF$ ) as

$$S_t^{(k)} \equiv \frac{2}{N^2} \left\langle \sum_{i=1}^{N-k} \cos[t s_i^{(k)}] \right\rangle. \quad (9)$$

This allows us to perform a *spectral distance decomposition of the SFF*, that is, write the complete SFF as composed of the  $k$ th neighbor SFFs,

$$S_t = \frac{1}{N} + \sum_{k=1}^{N-1} S_t^{(k)}, \quad (10)$$

where the first term originates from contributions of the zero frequencies [42].

Given a distribution  $\mathcal{P}^{(k)}(s)$  for the probability that the distance between a level and its  $k$ th neighbor is  $s$ , the ensemble-averaged  $knSFF$  reads

$$S_t^{(k)} = \frac{2(N-k)}{N^2} \int ds \mathcal{P}^{(k)}(s) \cos[ts]. \quad (11)$$

This expression assumes that the contribution of each spacing does not depend on the location in the spectrum, which gives the  $2(N-k)$  factor counting the number of  $k$ -neighbor distances in the spectrum. As we will show, the details of the distributions  $\mathcal{P}^{(k)}(s)$  and the number of energy levels accounted for are important to build up the ramp (or correlation hole); not only the nearest neighbor distribution,  $\mathcal{P}^{(1)}(s)$ , but also further correlations are crucial to get a *linear* ramp. In particular, assuming only nearest neighbor correlations results in a correlation hole but no linear ramp (see Section IV F).

In Section IV B, we show that the approximated distribution (4) yields a simple form to approximate the  $knSFF$  for the Gaussian ensembles, namely

$$S_t^{(k)} \approx \frac{2(N-k)}{N^2} e^{-\frac{\omega_k^2 t^2}{4\alpha}} \left[ \cos(\omega_k t) + \frac{1}{12\alpha} \omega_k t \left( \frac{\omega_k^2 t^2}{2\alpha} - 3 \right) \sin(\omega_k t) \right]. \quad (12)$$

Here,  $\alpha$  measures the amount of level repulsion and is given by (5), while the frequency is defined as

$$\omega_k^2 = \frac{\alpha}{2A_\alpha}. \quad (13)$$

So we find that the  $knSFF$  for each of the Gaussian ensembles can be written as a Gaussian envelope multiplied by an oscillating function. For increasing  $k$ , the number of oscillations increases, while their amplitude is being suppressed by the Gaussian decay. Interestingly, the frequency becomes linear for large enough  $k$ ,  $\omega_k \rightarrow k$ , such that summing up only the odd/even  $knSFF$ 's yields a resonance/anti-resonance at  $t = \pi$ . We find such resonances both for the folded and for the unfolded cases. By contrast, such resonances do not appear for the integrable case, which we turn to next. Figure 3 illustrates this phenomenon for XXZ with disorder, where we observe that this structure disappears as we increase the

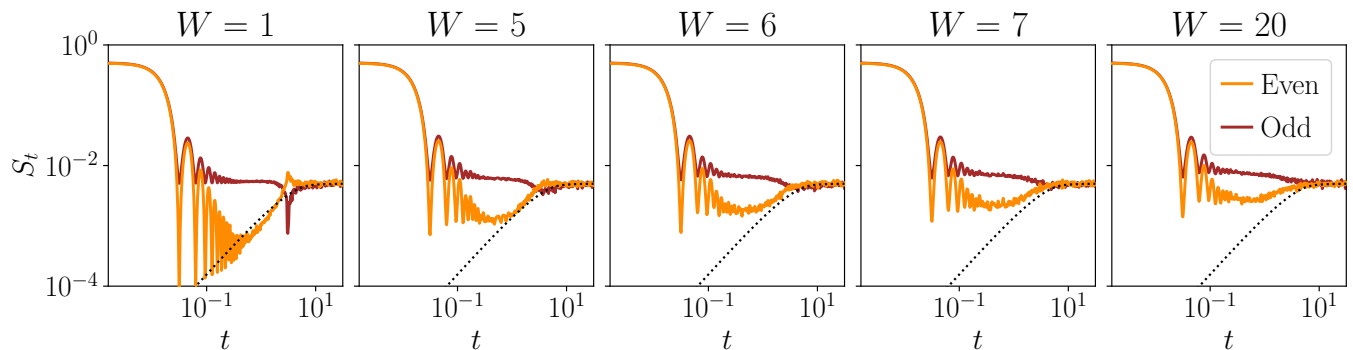


FIG. 3. **Even and Odd neighbor decomposition of the SFF** for the XXZ model along the chaos to integrability transition. Eq. (12) predicts a ‘resonance’ for the even contributions and an ‘anti-resonance’ for the odd contributions. The results have been averaged over  $N_{\text{av}} = 150$  realizations of the noise. The parameters are  $L = 16$ ,  $N_{\text{up}} = 8$ ,  $J_z = 2.21$ , and the system has periodic boundary conditions. The black dotted line shows the connected part of the SFF, detailed in App. D.

disorder. In Appendix E we show that this phenomenon is also present without unfolding the spectrum.

For the Poissonian (integrable) case, the exact result for the  $kn$ SFF reads

$$S_t^{(k)} = \frac{2(N-k) \cos(k \arctan t)}{N^2 (1+t^2)^{k/2}}. \quad (14)$$

Here, the oscillations in time die out fairly quickly because of the  $\arctan(t)$  term which saturates to  $\pi/2$ , in addition to the Lorentzian envelope becoming more and more suppressed with increasing  $k$ .

We now have the tools to ask how the correlation hole and ramp build up (or not) in different systems. This can be answered by introducing the *partial* SFF, which we define as

$$S_{t,K} \equiv \frac{1}{N} + \sum_{k=1}^K S_t^{(k)}, \quad (15)$$

and represents the SFF with a cut-off on the energy ranges contributing to it. Note that  $S_{t,N-1} = S_t$ . When it exists, the ramp incrementally builds up by adding up contributions  $S_t^{(k)}$  with larger range  $k$ . The partial SFF for different cut-offs is illustrated in Figures 4 and 5, respectively in the Poissonian and Gaussian random ensembles, and for the XXZ model with increasing disorder. We highlight the ‘dip time’, defined as the time for which  $S_{t,K}$  starts showing a ramp (and discussed in detail in App. C), and see how this time moves further to the left as the number of energy ranges is increased. In other words, the ramp builds up from the plateau time to the left, with smaller  $k$  contributing at late times and longer-range correlations needed to increase the duration of the linear ramp at early times. Along the same line, note that it is evident from the relationship between the two-level correlation function  $R_2(s) = \sum_{k=1}^{\infty} \mathcal{P}^{(k)}(s)$  and the probability densities  $\mathcal{P}^{(k)}(s)$  given in [43], see Appendix D, that small, medium, and large  $k$  neighbor probability distributions contribute to the structure of the SFF.

In Section IV A we expand on the relationship of the  $kn$ SFF decomposition for general autocorrelation functions.

### III. SPECTRAL STATISTICS

We now detail how to derive and characterize the  $k$ th neighbor distributions for Gaussian random matrix ensembles as well as for the Poissonian ensemble.

#### A. A surmise for the Gaussian random matrix ensembles

We look for the probability distribution of the  $k$ th level spacing,  $\mathcal{P}_\beta^{(k)}(s)$ . Let us start with  $k = 1$ . For a random matrix taken from a Gaussian ensemble (GOE, GUE or GSE), the nearest-neighbor level spacings  $\{s_i^{(1)}\}_{i=1}^{N-1}$  of the *unfolded spectrum* (see Appendix E) are well approximated by random variables taken from the *Wigner surmise* distribution,

$$\mathcal{P}_\beta^{(1)}(s) = C_{\beta,1} s^\beta e^{-A_{\beta,1} s^2}, \quad (16)$$

where  $C_{\beta,1}$  and  $A_{\beta,1}$  are constant in  $s$  and depend only on  $\beta$  (since  $k = 1$ ); they are set by the conditions that  $\mathcal{P}^{(1)}(s)$  is normalized and that the average level spacing is equal to unity,  $\langle s \rangle = \int_0^\infty s \mathcal{P}^{(1)}(s) ds = 1$ .

This result can be derived by considering the distribution of the spacing  $|E_2 - E_1|$  between the eigenenergies of a  $2 \times 2$  random matrix, which is the smallest possible random matrix to have a nearest-neighbor spacing. As Wigner rightly conjectured [7], this is a good approximation to the level spacing distribution also for matrices with  $N > 2$ ; the distribution of nearest-neighbor level spacings in a Gaussian random matrix of any size very closely follows his surmise, provided that the spectrum is unfolded. For exact results at  $N = 3$ , see e.g. [44, 45].

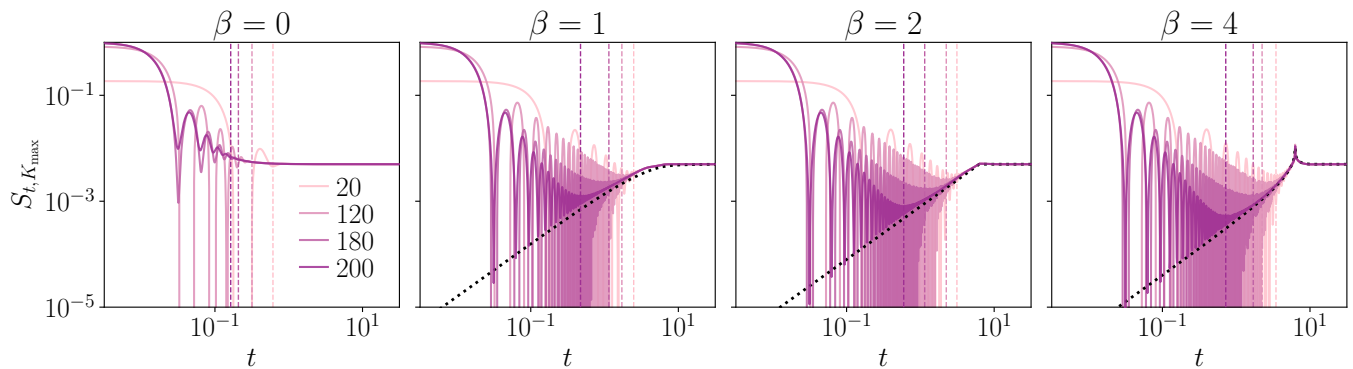


FIG. 4. **Spectral distance decomposition of Spectral Form Factor** for Random Matrix summing the first  $K_{\max} = 20, 120, 180, 200$  spectral distances for Poisson, GOE, GUE and GSE. Dip time (dashed line). The results are computed by summing the approximated analytics. The black dotted line shows the connected part of the SFF, as detailed in App. D.

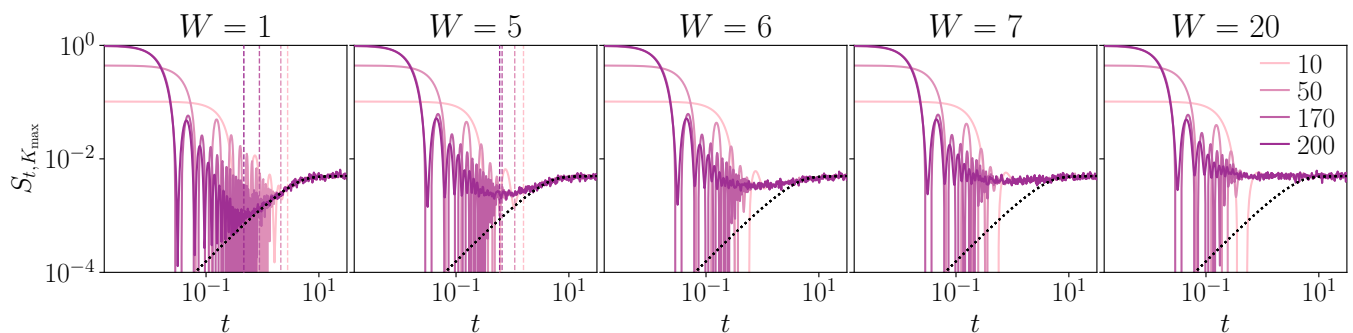


FIG. 5. **Spectral distance decomposition of Spectral Form Factor** for XXZ model summing the first  $K_{\max} = 10, 50, 170, 200$  spectral distances. The black dotted line shows the connected part of the SFF for GOE, see App. D. The results have been averaged over  $N_{\text{av}} = 150$  disorder realizations. The parameters are  $L = 16$ ,  $N_{\text{up}} = 8$ ,  $J_z = 2.21$ , and the system has periodic boundary conditions.

For energy levels further apart, we follow Wigner's footsteps and use the smallest possible random matrix ensemble with that particular spectral distance. Specifically, to find the distribution of the  $k$ th neighbor level spacing,  $s^{(k)}$ , we use an  $N = k + 1$  dimensional random matrix with energy levels  $E_1 \leq E_2 \leq \dots \leq E_{k+1}$  and look for the distribution

$$\mathcal{P}_\beta^{(k)}(s) = \int_{-\infty}^{\infty} dE_1 \int_{E_1}^{\infty} dE_2 \cdots \int_{E_k}^{\infty} dE_{k+1} \rho(E_1, \dots, E_{k+1}) \times \delta[s - (E_{k+1} - E_1)], \quad (17)$$

where  $\rho$  is the joint probability distribution (1), and where we have written the integration limits explicitly, taking into account the ordering of the levels.

Following the derivation in [44], we change variables from  $\{E_1, E_2, \dots, E_{k+1}\}$  to  $\{E_1, s_1, s_2, \dots, s_k\}$ , where  $s_i \equiv s_i^{(1)}$  are all the nearest-neighbor spacings. So

$$\mathcal{P}_\beta^{(k)}(s) \propto \int_{-\infty}^{\infty} dE_1 \int_0^{\infty} ds_1 \cdots \int_0^{\infty} ds_k \rho(E_1, s_1, \dots, s_k) \times \delta\left(s - \sum_{i=1}^k s_i\right), \quad (18)$$

where we omit the constant Jacobian which is not relevant in this work because we will eventually normalize the final result. Notice that  $E_1$  appears only in the exponential term of  $\rho(E_1, s_1, \dots, s_k) = [p(s_1, s_2, \dots, s_k)]^\beta \times e^{-A[E_1^2 + (E_1 + s_1)^2 + (E_1 + s_1 + s_2)^2 + \dots + (E_1 + s_1 + \dots + s_k)^2]}$ , written here with the  $k(k+1)/2$  degree polynomial

$$p(s_1, s_2, \dots, s_k) = s_1(s_1 + s_2) \cdots (s_1 + s_2 + \dots + s_k) \times s_2(s_2 + s_3) \cdots (s_2 + s_3 + \dots + s_k) \times \cdots \times s_{k-1}(s_{k-1} + s_k) \times s_k. \quad (19)$$

Since  $s_i \geq 0$  for all  $i$ , this polynomial is positive everywhere. Performing the Gaussian integral over  $E_1$ , we find (up to an irrelevant constant)

$$\mathcal{P}_\beta^{(k)}(s) \propto \int_0^{\infty} ds_1 \cdots \int_0^{\infty} ds_k [p(s_1, s_2, \dots, s_k)]^\beta \times e^{-Aq(s_1, \dots, s_k)} \delta\left(s - \sum_{i=1}^k s_i\right), \quad (20)$$

where we defined the quadratic polynomial resulting from

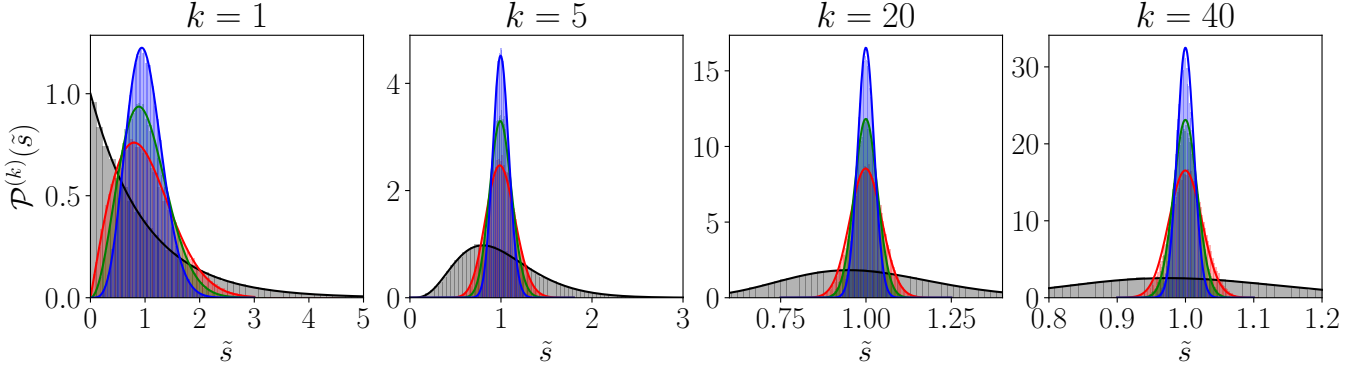


FIG. 6.  $k$ -th neighbor level spacing distribution for the Poisson (black), GOE (red), GUE (green), and GSE (blue) ensembles for different spectral distances  $k = 1, 5, 20, 40$ . The data and the analytics are rescaled as  $\tilde{s} = s/k$  for ease of plotting, and thus the average of all distributions is always located at 1. The analytical Wigner surmise (lines), Eqs. (7) and (4), is in good agreement with the unfolded numerical data (histogram). Numerical results are obtained averaging over  $N_{\text{av}} = 1000$  realizations of random matrices of dimension  $N = 100$ .

the integration over  $E_1$  as

$$q(\{s_i\}) = \sum_{i=1}^k \frac{i(k+1-i)}{k+1} s_i^2 + \sum_{i<j=1}^k \frac{2i(k+1-j)}{k+1} s_i s_j. \quad (21)$$

Note that since  $s_i \geq 0$  for all  $i$  and the coefficients of this quadratic polynomial are always positive, we have  $q(s_1, \dots, s_k) \geq 0$  everywhere. Next, we rescale the spacings through  $x_i = s_i/s$ . Taking into account the Jacobian of this transformation, which is  $s^k$ , the homogeneity of  $p(s_1, \dots, s_k)$  and of  $q(s_1, \dots, s_k)$ , and using the delta function identity  $\delta(ax) = \delta(x)/|a|$ , we arrive at

$$\mathcal{P}_\beta^{(k)}(s) \propto s^{k-1} s^{\frac{k(k+1)}{2}\beta} \int_0^\infty dx_1 \cdots \int_0^\infty dx_k \quad (22)$$

$$\times [p(x_1, x_2, \dots, x_k)]^\beta e^{-As^2 q(x_1, \dots, x_k)} \delta\left(1 - \sum_{i=1}^k x_i\right).$$

This is an integral over a  $(k-1)$  simplex. Using the  $\delta$ -function to set  $x_k = 1 - x_1 - x_2 - \dots - x_{k-1}$  and restricting the integration limits, we replace the quadratic function by  $\bar{q}(\{x_i\}_{i=1}^{k-1}) = \frac{k}{k+1} - 2 \sum_{i=1}^{k-1} B_i x_i + \sum_{i,j=1}^{k-1} A_{ij} x_i x_j$  and detail the elements of the vector  $\mathbf{B}$  and the matrix  $\mathbf{A}$  being detailed in Appendix B; at the same time, we denote the change of the polynomial  $p(\{x_i\}_{i=1}^k)$  as  $\bar{p}(\{x_i\}_{i=1}^{k-1})$ . After completing the square, we arrive at the  $(k-1)$ -dimensional integral

$$\mathcal{P}_\beta^{(k)}(s) \propto s^{\frac{k(k+1)}{2}\beta} s^{k-1} e^{-\frac{A}{2}s^2} \quad (23)$$

$$\times \int_0^1 dx_1 \int_0^{1-x_1} dx_2 \cdots \int_0^{1-\sum_{i=1}^{k-2} x_i} dx_{k-1}$$

$$\times [\bar{p}(x_1, x_2, \dots, x_{k-1})]^\beta e^{-As^2(\mathbf{x}^T - \mathbf{m}^T)\mathbf{A}(\mathbf{x} - \mathbf{m})},$$

where  $\mathbf{m} = \mathbf{A}^{-1}\mathbf{B}$  and where we have used  $A[\frac{k}{k+1} - \mathbf{B}^T\mathbf{A}^{-1}\mathbf{B}] = A/2$  for all  $k$ . It can be verified that  $\mathbf{m}$

simplifies to  $(1/2, 0, \dots, 0)$  which means that the Gaussian is centered at zero for all  $x_i$  except  $x_1$ .

The integral over the simplex is challenging to compute exactly. For small  $s$  the Gaussian in the integral can be expanded to second order in  $s$ , resulting in a correction to the width of the pre-factor Gaussian function, while at large  $s$  the integral gives corrections to the power law (as we discuss below).

We can thus approximate the distribution of  $knLS$  by (4) with  $\alpha$  given in (5) and  $A_\alpha, C_\alpha$  set by the normalization conditions resulting from the unfolding process, see Eqs. (25) below. Note that  $\alpha_{\beta,k} \in \mathbb{N}$  for the all possible  $k = 1, 2, \dots, N-1$  and  $\beta \in \mathbb{N}$ .

Since similar results have been reported in the literature, let us review their argument to contextualize our derivation. The first generalization of Wigner surmise that we are aware of assumes a Brody-like ansatz, which essentially leaves the power-law  $\alpha$  as a free parameter [35]. In Ref. [46], the power-law in (5) is found using a small  $s$  expansion and the generalized Wigner surmise, Eq. (4), is obtained assuming a Gaussian behavior at large  $s$ . This approach is also followed in [38] in the context of 2D Poisson point processes. These references thus find the same distribution through heuristic arguments. Formal results for the  $knLS$  probability distribution can be obtained exactly using tools from RMT, see e.g. [2], and there are even connections between the different  $knLS$  distributions [39]. Since these results are formal and exact, they lack an explicit expression for the  $knLS$  distribution reminiscent of the Wigner surmise, which is itself an approximation [3]. More recently, an extension of these results to spacing ratios was tested numerically [37] but with no analytical proof. Lastly, Rao [34] claims to have an analytic derivation of the generalized Wigner distribution from the joint probability density of eigenvalues. However, since the energies are not ordered, the spacing  $E_{k+1} - E_1$  need not be a  $k$ th spacing. In turn, our derivation gives a derivation based on Wigner's original

argument, i.e. considering the joint probability density of eigenvalues of the largest possible matrix with a  $k$ -th spacing; we have explicitly stated the approximations involved in getting the generalized Wigner distribution and discuss the corrections to the distribution below.

The generalized Wigner surmise (4) has been obtained starting from the joint probability distribution of eigenvalues (1)—without unfolding. It gives a good approximation of the  $knLS$  distribution for small  $k$ , provided that the spectrum is unfolded. As in the case of Wigner’s surmise (16), unfolding the spectrum sets the constants  $A_{\beta,k}$  and  $C_{\beta,k}$  from the conditions

$$\int_0^\infty \mathcal{P}_\beta^{(k)}(s) ds = 1, \quad (24a)$$

$$\int_0^\infty s \mathcal{P}_\beta^{(k)}(s) ds = k. \quad (24b)$$

The first condition normalizes the distribution, while the second condition fixes the average spacing between a level and its  $k$ th neighbor to equal  $k$ . The constants can be found to be

$$A_\alpha = \left[ \frac{\Gamma(\frac{\alpha}{2} + 1)}{k \Gamma(\frac{\alpha+1}{2})} \right]^2 \quad (25a)$$

$$C_\alpha = \frac{2}{\Gamma(\frac{\alpha+1}{2})} \left[ \frac{\Gamma(\frac{\alpha}{2} + 1)}{k \Gamma(\frac{\alpha+1}{2})} \right]^{\alpha+1}, \quad (25b)$$

where  $\alpha$  is given in Eq. (5) and depends on  $\beta$  and on  $k$ . Fig. 6 shows that our analytical results (4) capture the numerical simulation for all matrices of the Gaussian ensembles.

Expanding the expressions (25a) and (25b) in large  $\alpha$  provides approximations for  $A_\alpha$  and  $C_\alpha$  that work particularly well when comparing with numerical results:

$$A_\alpha \approx \frac{1}{k^2} \left( \frac{\alpha}{2} + \frac{1}{4} + \frac{1}{16\alpha} \right), \quad (26a)$$

$$C_\alpha \approx \frac{1 + 12\alpha}{12\sqrt{\pi\alpha} k^{1+\alpha}} e^{\frac{1}{4} + \frac{\alpha}{2}}. \quad (26b)$$

From (24b), the distribution  $\mathcal{P}^{(k)}(s)$  has average  $\langle s \rangle = k$ , and its variance is therefore

$$\Delta_\beta^{(k)} \equiv \langle s^2 \rangle - \langle s \rangle^2 = \left( \frac{\alpha + 1}{2A_\alpha} \right) - k^2. \quad (27)$$

This result is illustrated in Fig. 1. As mentioned in Sec. II, the variance of the exact distributions follows Eq. (6). *Corrections at large  $s$ .*—As mentioned, we expect corrections to the generalized Wigner surmise (4) at large  $s$ . Starting back from Eq. (23), we can bound the resulting integral by a saddle-like approximation, namely, replacing  $\bar{p}(x_1, x_2, \dots, x_{k-1})$  by its maximum  $\bar{p}_{max}$  over the simplex. Since, at large  $s$ , the Gaussian has a very narrow peak (located on the boundary of the simplex), we can take the limits to infinity; the integral thus introduces an  $s$ -dependence of  $(1/s)^{k-1}$ . The probability

distribution has a resulting  $s$ -dependence for large  $s$  corrected as

$$\mathcal{P}_\beta^{(k)}(s) \xrightarrow{s \rightarrow \infty} s^{\frac{k(k+1)}{2}\beta} e^{-\frac{1}{2}As^2}. \quad (28)$$

Note that the behaviour at large  $s$  is not the same as the behaviour at large  $k$ , as diagnosed for example by (6), for which we would need further work to account for.

Note that, since the power  $\frac{k(k+1)}{2}\beta$  is linear in  $\beta$ , this distribution can be interpreted as the Boltzmann factor of a Coulomb or ‘log gas’ [47, 48], which models a 1-dimensional array of atoms in a harmonic trap interacting with an effective potential taken as a logarithmic function of their distance. This interpretation as a log gas does not hold for the  $\alpha$  coefficient in (5) because of zero-th order terms in  $\beta$  that would need to be canceled out with temperature-dependent interaction strengths in the effective model.

## B. ‘Poisson’ ensemble: uncorrelated energy levels

We revisit the  $k$ th neighbor distribution for ensembles with uncorrelated energy levels, which we label with  $\beta = 0$  for convenience. This is known in the literature as the ‘Poissonian’ case whose nearest-neighbor spectral statistics satisfy  $\mathcal{P}^{(1)}(s) = e^{-\bar{\rho}s}$ , where  $\bar{\rho}$  is the average density of states, taken to be the uniform distribution  $\bar{\rho}(E) = \bar{\rho} = 1$ . Assuming no correlations whatsoever between the energies, the joint probability distribution of the set of (uncorrelated) nearest-neighbor differences  $\{s_1, s_2, \dots, s_k\}$  is just a product of the individual distributions,

$$P(s_1, s_2, \dots, s_k) = P(s_1)P(s_2) \dots P(s_k) = e^{-\sum_{i=1}^k s_i}. \quad (29)$$

As in the case of the Gaussian ensembles, the joint distribution  $P(s_1, s_2, \dots, s_k)$  allows us defining the probability that the  $k$ th nearest neighbor spacing is  $s$  as

$$\mathcal{P}_0^{(k)}(s) \propto \int_0^\infty ds_1 \dots ds_k P(\{s_i\}_{i=1}^k) \delta(s - \sum_{i=1}^k s_i). \quad (30)$$

This integral can also be carried out using rescaled variables  $x_i = s_i/s$ . The Jacobian brings a factor  $s^k$  and the integration over the delta function contributes a  $s^{-1}$  and sets everywhere  $x_k = 1 - \sum_{i=1}^{k-1} x_i$ . This yields

$$\begin{aligned} \mathcal{P}_0^{(k)}(s) &\propto s^{k-1} e^{-s} \int_0^1 dx_1 \int_0^{1-x_1} dx_2 \dots \int_0^{1-\sum_{i=1}^{k-2} x_i} dx_{k-1} \\ &= s^{k-1} e^{-s} \times \text{constant}, \end{aligned} \quad (31)$$

where the second equality follows from the fact that the integral over the simplex is a finite constant. The normalized distribution follows as

$$\mathcal{P}_0^{(k)}(s) = \frac{1}{(k-1)!} s^{k-1} e^{-s}.$$

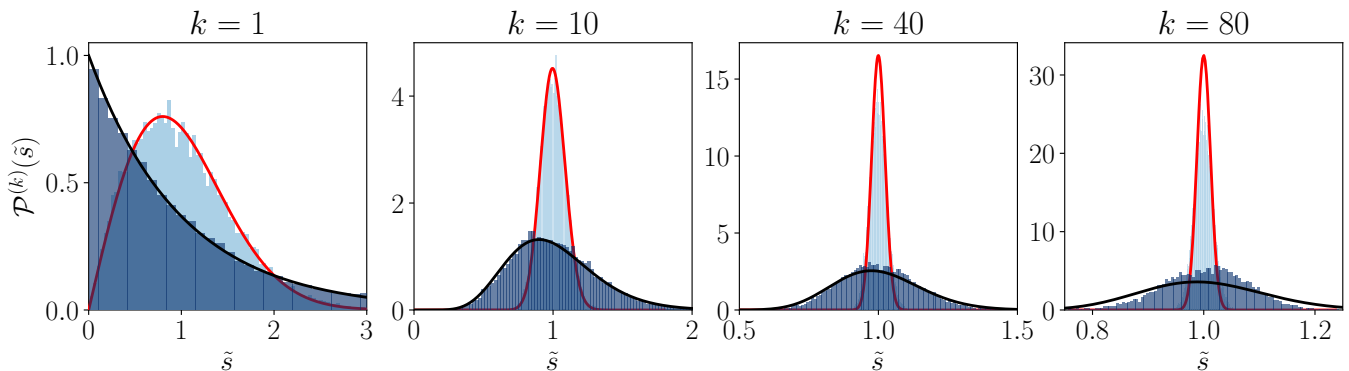


FIG. 7.  $k$ -th neighbor level spacing distribution in XXZ for spectral neighbors,  $k = 1, 10, 40, 80$ , in the chaotic  $W = 1$  (light blue) and integrable  $W = 20$  (dark blue) phases along with the analytical results for Poisson (black line) and GOE (red line) models. The plot shows the rescaled spacing  $\tilde{s} = s/k$ . The deviation between the integrable phase and Poissonian starts to be seen at  $k = 35$  and is very apparent at  $k = 70$  where the numerical distribution is much narrower. The considered XXZ model has  $L = 16$  spins in the zero magnetization sector  $N_u = 8$ , the hopping is  $J_z = 2.21$ , with PBC, the energy window size is  $N_{\text{en}} = 200$  and the results include  $N_{\text{av}} = 50$  disorder realizations. The variance of the distribution as function of  $k$  is given in Fig. 2.

This distribution is illustrated in Fig. 6. We verify that the average value is  $\langle s \rangle = k$ , as expected. Note that although for  $k \geq 2$ , the probability for very small  $k$ th spacing goes to zero, this does not reflect ‘level repulsion’ but rather reflects the fact that there is a small probability of having two levels that have  $k - 2$  levels between them be very close together. It is worth noting that this contrast with the behavior in Gaussian ensembles, where the ‘repulsion’ of two such levels is much stronger and goes as  $s^{k-1 + \frac{k(k+1)}{2}\beta}$ .

The variance of the  $kn$ LS distribution for the Poissonian ensemble is  $\Delta_0^{(k)} = k$ , as mentioned in Eq. (8). Comparing this result with the large  $k$  behavior of  $\Delta_\beta^{(k)}$  (6), we see that the Gaussian ensemble  $k$ th neighbor distributions are much more narrow than those of the completely uncorrelated (Poissonian) ensemble. Thus, as mentioned in the summary, the variance is a good indicator of the strength of spectral correlations—also *c.f.* Fig. 2.

### C. Spectral statistics in the disordered XXZ model

To study the correlations in the spectrum of the XXZ spin chain with disorder and their dynamical signatures, we average over many realizations of its Hamiltonian  $\hat{H} = \hat{H}_{\text{XXZ}} + H_{\text{dis}}$  for each value of  $W$  and focus on a window in the densest part of the spectrum, upon which we perform global unfolding using a polynomial fit. The procedure is detailed in App. E.

Figure 7 shows results for the rescaled distributions  $\mathcal{P}^{(k)}(\tilde{s})$  for different spectral distances  $k$  in the model’s chaotic ( $W = 1$ ) and integrable ( $W = 20$ ) phases. The results from the random matrices relevant to each phase, respectively the GOE (Eq. (4) with  $\beta = 1$ ) and Poissonian (8), are illustrated for comparison. Small devia-

tions appear for larger  $k$ . Those deviations between the physical model and idealized random matrices are better characterized by the variances of the distributions  $\mathcal{P}^{(k)}(s)$ , presented above in Figure 2, and extracted from numerical data for the disorder XXZ spin chain. Up to a certain value of  $k$  both the chaotic and integrable phases follow the expected GOE and Poisson behavior, respectively. For larger  $k$  we find deviations in both phases, particularly noticeable for the integrable phase, which can be understood as follows.

For large disorder, the dominant contribution to the Hamiltonian is  $\hat{H}_{\text{dis}}$ , which on its own, can be thought of as a free, non-interacting Hamiltonian with energy levels given by  $E_i = \sum_{n=1}^L \pm h_n^z$ , with  $i = 1, 2, \dots, N$ . In the zero magnetization sector in which we are working, there are as many pluses as minuses. The energy level structure can be understood by ordering the  $h_n^z$  according to their absolute value. Then, the lowest energy level is obtained by distributing the  $\pm$  such as to attribute minuses to the  $|h_n^z|$  with larger values and pluses to the  $|h_n^z|$  with smaller values. The highest energy level has the same structure but with pluses and minuses flipped. This small exercise shows that energy levels which are far away are actually correlated in  $\hat{H}_{\text{dis}}$ , thus explaining the deviation from Poissonian statistics observed in Figures 2 and 7.

## IV. DYNAMICAL SIGNATURES OF CHAOS

In this section we turn to the effect of spectral statistics on dynamical quantities, focusing on the SFF. We introduce the  $k$ th neighbor SFFs and study their properties. We then sum them up (with appropriate coefficients) to obtain the complete SFF. In this process, we learn about the underlying structure which can be unveiled via the decomposition of the SFF into  $kn$ SFF components.

### A. The ensemble averaged $k$ th neighbor SFF

The spectral form factor (SFF) is a time- and temperature-dependent quantity that probes the spectrum of a given quantum system. For a system at inverse temperature  $\tilde{\beta}$ , it can be defined as  $\mathcal{S}_t(\tilde{\beta}) = |Z(\tilde{\beta} + it)/Z(\tilde{\beta})|^2$ , with the partition function  $Z(\tilde{\beta}) = \sum_{i=1}^N e^{-\tilde{\beta}E_i}$  including all the energies  $\{E_i\}_{i=1}^N$  of the Hamiltonian's spectrum ( $N$  can be infinite). In more detail,

$$\mathcal{S}_t(\tilde{\beta}) = \frac{\sum_{i,j=1}^N e^{-\tilde{\beta}(E_i+E_j)} e^{-it(E_i-E_j)}}{\sum_{i,j=1}^N e^{-\tilde{\beta}(E_i+E_j)}}. \quad (32)$$

In the infinite temperature limit,  $\tilde{\beta} \rightarrow 0$ , the SFF becomes

$$\mathcal{S}_t(0) \equiv \mathcal{S}_t = \frac{N + 2 \sum_{i>j} \cos[t(E_i - E_j)]}{N^2}, \quad (33)$$

whose numerator can be divided into terms according to spectral distances  $s_i^{(k)}$ . This decomposition of the SFF is thus

$$\mathcal{S}_t = \frac{1}{N} + \sum_{k=1}^{N-1} \mathcal{S}_t^{(k)}, \quad (34)$$

and is formed by summing the  $k$ -th neighbor spectral form factors (knSFFs)

$$\mathcal{S}_t^{(k)} \equiv \frac{2}{N^2} \sum_{i=1}^{N-k} \cos[t s_i^{(k)}]. \quad (35)$$

As mentioned, the SFF is not self-averaging [22]; so we wish to compute the ensemble average  $S_t = 1/N + \sum_{k=1}^{N-1} \langle \mathcal{S}_t^{(k)} \rangle$ , which boils down to computing the ensemble average of the individual contributions from each spectral distance,  $\langle \mathcal{S}_t^{(k)} \rangle \equiv S_t^{(k)}$ —also introduced earlier in the main results, Eq. (10). We show below a series of approximations that allow us to derive an analytical expression for the  $S_t^{(k)}$  which provides a good approximation and is obtained starting from the distributions  $\mathcal{P}^{(k)}$  derived in Section III.

As discussed above, the ensemble average of the SFF can be decomposed according to the contributions from the various spectral spacings  $k$ . The latter can themselves be decomposed according to the energy levels  $i$  as

$$S_t^{(k)} = \frac{2}{N^2} \sum_{i=1}^{N-k} \int dE_1 \dots dE_N \rho(\{E_i\}) \cos[t s_i^{(k)}]. \quad (36)$$

Note that the energies  $E_i$  are ordered. In the first step, we approximate all energy spacings  $s_i^{(k)} = E_{i+k} - E_i$  as being independent of the absolute energy level [49] and set  $i = 1$  as the reference level, so  $s_i^{(k)} \rightarrow s_1^{(k)}$  and the sum over  $i$  just becomes an  $(N - k)$  factor. Then, in the

same spirit as the  $knLS$  distribution, we use the largest possible matrix which describes the  $k$  level spacings and take  $N \rightarrow (k + 1)$ . We recognize the distribution of the  $knLS$ , Eq. (17), and the  $knSFF$  (36) becomes

$$\begin{aligned} S_t^{(k)} &\approx \frac{2(N-k)}{N^2} \int ds^{(k)} \mathcal{P}^{(k)}(s^{(k)}) \cos[t s^{(k)}], \\ &\equiv C_N^{(k)} f_t^{(k)}, \end{aligned} \quad (37)$$

where in the second line, we have introduced the following function and constant for later notational convenience:

$$f_t^{(k)} \equiv \int ds \mathcal{P}^{(k)}(s) \cos(t s) \quad (38a)$$

$$C_N^{(k)} \equiv \frac{2(N-k)}{N^2}. \quad (38b)$$

Let us mention that this result can be generalized to quantities related to the SFF, such as autocorrelation functions. Indeed, the autocorrelation function at infinite temperature of a Hermitian operator  $\hat{O} = \hat{O}^\dagger$  (i.e. any observable) can be decomposed in a similar manner using  $f_t^{(k)}$  and changing only the coefficients  $C_N^{(k)}$ , as follows. Consider the autocorrelation function:

$$\mathcal{C}_t \equiv \frac{\text{Tr}(\hat{O}\hat{O}(t))}{\text{Tr}(\hat{O}^2)} = \frac{1}{\mathcal{N}^2} \sum_{i,j=1}^N |O_{ij}|^2 \cos[(E_i - E_j)t], \quad (39)$$

where  $O_{ij}$  are the matrix elements of the operator  $\hat{O}$  in the energy basis and  $\mathcal{N}^2 = \sum_{i,j=1}^N |O_{ij}|^2$ . The ensemble average of  $\mathcal{C}_t$  can be decomposed into  $k$ th neighbor autocorrelation functions (see Appendix I for more details) as

$$\mathcal{C}_t^{(k)} \equiv O_N^{(k)} f_t^{(k)}, \quad (40)$$

where  $f_t^{(k)}$  are defined in (38a) and we define the coefficients:

$$O_N^{(k)} \equiv \frac{2}{\mathcal{N}^2} \sum_{i=1}^{N-k} |O_{i,i+k}|^2. \quad (41)$$

An explicit relation between correlation functions and the  $knSFF$ 's, along with a possible dissipative protocol to measure them, will be detailed in Sec. V.

We now turn to derive analytical expressions for  $f_t^{(k)}$  (and for  $S_t^{(k)}$ ) for the GOE, GUE and GSE as well as for completely uncorrelated energy levels (Poissonian ensemble).

### B. The $knSFF$ in Gaussian random matrix ensembles

#### 1. Analytical results

With the approximated analytical result for  $\mathcal{P}^{(k)}(s)$  obtained in (4), we can look for an expression of the

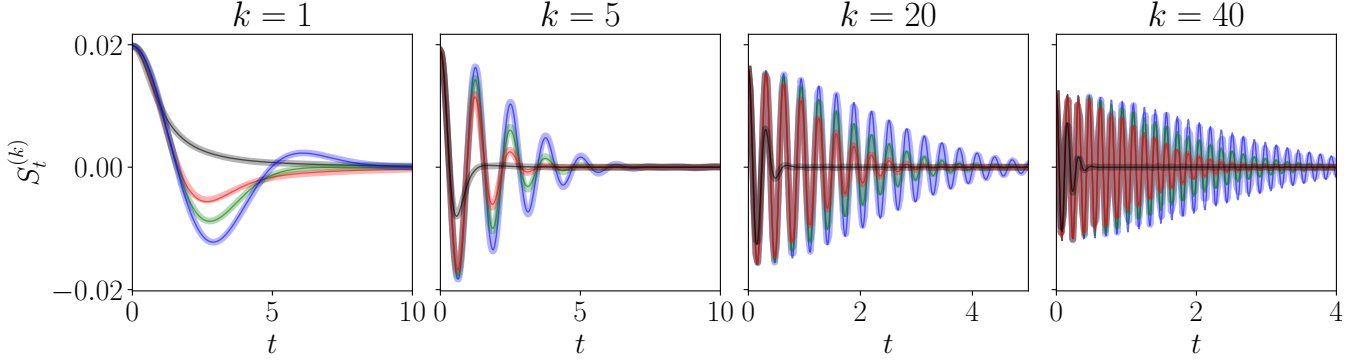


FIG. 8. **Time evolution of the knSFF** for Poisson (black), GOE (red), GUE (green) and GSE (blue) for different spectral neighbors,  $k = 1, 5, 20, 40$  in systems of dimension  $N = 100$ . The plots for  $k = 5, 20, 40$  show analytical results (thin lines) from (14) and (12), while for  $k = 1$  we show the exact expression (47), and numerical results for random matrices averaged over  $N_{\text{av}} = 1000$  realizations (thick transparent lines). While we do not expect the approximation (12) to be good for small  $k$ , it works already quite well for GSE and  $k = 1$  and less so for GUE and GOE, in that order. Note the different scales in the time axis, chosen to better represent the increasing number of oscillations with the spectral neighbor  $k$ , see Eq. (55).

knSFF  $S_t^{(k)}$  for the Gaussian random matrix ensembles, starting from (37):

$$f_t^{(k)} \equiv \int_0^\infty ds \mathcal{P}^{(k)}(s) \cos(ts) = \sum_{n=0}^{\infty} \frac{(-1)^n}{(2n)!} t^{2n} \langle s^{2n} \rangle \quad (42)$$

where

$$\langle s^{2n} \rangle = \int_0^\infty ds s^{2n} \mathcal{P}^{(k)}(s) = \left( \frac{\alpha+1}{2} \right)_n (A_\alpha)^{-n} \quad (43)$$

where we have used the Pochhammer symbol  $(a)_n = a(a+1)\dots(a+n-1) = \Gamma(a+n)/\Gamma(a)$ . In turn, the function becomes

$$f_t^{(k)} = \sum_{n=0}^{\infty} \frac{\left(\frac{\alpha+1}{2}\right)_n}{(1/2)_n} \frac{(-t^2/4A_\alpha)^n}{n!}. \quad (44)$$

This sum can be expressed in terms of a hypergeometric function

$$f_t^{(k)} = e^{-\frac{t^2}{4A_\alpha}} {}_1F_1\left(-\frac{\alpha}{2}; \frac{1}{2}; \frac{t^2}{4A_\alpha}\right). \quad (45)$$

Since the coefficient  $1/(2\sqrt{A_\alpha})$  appears in the  $t$ -dependent exponent, it is homogeneous to a frequency  $\omega_k$ . We thus set

$$\frac{1}{2A_\alpha} \equiv \frac{\omega_k^2}{\alpha}, \quad (46)$$

and we will see that this quantity sets the width of the Gaussian envelope. The hypergeometric function can itself be expressed in terms of a Laguerre function, so we get

$$\begin{aligned} f_t^{(k)} &= e^{-\frac{1}{2\alpha}\omega_k^2 t^2} {}_1F_1\left(-\frac{\alpha}{2}; \frac{1}{2}; \frac{\omega_k^2 t^2}{2\alpha}\right) \\ &= \sqrt{\frac{\pi\alpha}{2}} \frac{k}{\omega_k} e^{-\frac{\omega_k^2 t^2}{2\alpha}} L_{\alpha/2}^{-1/2}\left(\frac{\omega_k^2 t^2}{2\alpha}\right). \end{aligned} \quad (47)$$

The Laguerre function,  $L_\mu^a$  with  $m-1 < \mu < m$  for  $m \in \mathbb{N}$  and  $a > -1$ , is defined by the infinite sum [50]

$$L_\mu^a(z) = \sum_{k=0}^{\infty} \binom{\mu+a}{\mu-k} \frac{(-z)^k}{k!}. \quad (48)$$

When  $\alpha$  is even,  $\alpha = 2m$  for  $m \in \mathbb{N}$ , in (47), the Laguerre function becomes a Laguerre polynomial of degree  $m$ :

$$L_m^a(z) = \sum_{k=0}^m \binom{m+a}{m-k} \frac{(-z)^k}{k!}. \quad (49)$$

Since the degree of the Laguerre polynomial (or function, for non integer  $\alpha/2$ ) grows quadratically with  $k$ , we can use the approximation for Laguerre polynomial of high degree [51]:

$$\begin{aligned} L_n^a(x) &= \frac{n^{a/2-1/4}}{\sqrt{\pi x^{a/2+1/4}}} e^{x/2} \left[ \cos(\theta_{a,n}(x)) \left(1 + \mathcal{O}\left(\frac{1}{n}\right)\right) \right. \\ &\quad \left. + \sin(\theta_{a,n}(x)) \left(\frac{b_a(x)}{\sqrt{n}} + \mathcal{O}\left(\frac{1}{n}\right)\right) \right] \end{aligned} \quad (50)$$

where  $\theta_{a,n}(x) = 2\sqrt{nx} - a\pi/2 - \pi/4$  and  $b_a(x) = (4x^2 - 12a^2 - 24ax - 24x + 3)/(48\sqrt{x})$ . Note that  $b_{-1/2}(x) = \frac{\sqrt{x}}{12}(x-3)$ .

In our case, we have a Laguerre polynomial of degree  $n = \alpha/2$  (not necessarily integer),  $a = -1/2$  and  $x = \frac{\omega_k^2 t^2}{2\alpha}$ , so the above approximation reads

$$L_{\frac{\alpha}{2}}^{-\frac{1}{2}}(x) \approx \sqrt{\frac{2}{\pi\alpha}} e^{\frac{x}{2}} \left[ \cos(\omega_k t) + \frac{b_{-\frac{1}{2}}(x)}{\sqrt{\alpha/2}} \sin(\omega_k t) \right]. \quad (51)$$

As can be seen in (50), the terms in the square brackets of (51) are an approximation up to (not including)  $\mathcal{O}(1/\alpha)$ . Thus, when plugging this result into (47) we must make

sure that the combined coefficient of the square brackets is expanded to the same order in  $\alpha$

$$\frac{1}{\sqrt{\alpha/2}} \frac{\Gamma(\alpha/2 + 1)}{\Gamma(\alpha/2 + 1/2)} = 1 + \mathcal{O}(1/\alpha). \quad (52)$$

Eventually, we find that  $f_t^{(k)}$  can be approximated by [52]

$$f_t^{(k)} = \left(1 + \mathcal{O}(1/\alpha)\right) e^{-\frac{\omega_k^2 t^2}{4\alpha}} \times \left[ \cos(\omega_k t) + \sqrt{\frac{2}{\alpha}} b_{-\frac{1}{2}} \left( \frac{\omega_k^2 t^2}{2\alpha} \right) \sin(\omega_k t) + \mathcal{O}(1/\alpha) \right], \quad (53)$$

We note that the frequency is well approximated at large  $k$  by a linear function in  $k$ :

$$\omega_k \approx k - \frac{1}{2\beta k} + \mathcal{O}(1/k^2). \quad (54)$$

Let us make several remarks about expression (53):

- The initial value is always equal to unity,  $f_{t=0}^{(k)} = 1$  for all  $k$ ;
- For  $t \rightarrow \infty$ , the overall exponential factor,  $e^{-\frac{\omega_k^2 t^2}{4\alpha}}$ , makes  $f_t^{(k)} \rightarrow 0$ ;
- $f_t^{(k)}$  is expressed as a sum of a cosine and a sine with the same frequency  $\omega_k \rightarrow k$  at large  $k$ ;
- Apart from the overall exponential factor, the coefficient of  $\cos(\omega_k t)$  is 1 while the coefficient of  $\sin(\omega_k t)$  is time-dependent and is equal to  $\sqrt{\frac{2}{\alpha}} b_{-1/2} \left( \frac{\omega_k^2 t^2}{2\alpha} \right) = \frac{1}{12\alpha} \omega_k t \left( \frac{\omega_k^2 t^2}{2\alpha} - 3 \right)$ . It is of  $\mathcal{O}(1/k)$  and thus of less consequence for large  $k$ . Note that, at the same time, it is more significant at large  $t$ . This is compatible with the fact that small  $k$  terms (corresponding to low frequencies) are more significant at long time scales.
- We can compute the number of oscillations in one standard deviation of the envelope  $\sqrt{2\alpha}/\omega_k$ , by comparing it with the period of the oscillations  $T_k = 2\pi/\omega_k$ . We thus find

$$\frac{\sqrt{2\alpha}}{2\pi} \xrightarrow[k \rightarrow \infty]{} \frac{\sqrt{\beta}}{2\pi} k. \quad (55)$$

So the number of oscillations of the  $kn$ SFF in the envelope is proportional to  $\sqrt{\alpha}$ , and scales linearly with the neighbor degree  $k$  for large  $k$ , as illustrated in Fig. 8. The figure also illustrates that the largest number of oscillations that happen before the signal flattens because of the exponential decays is for the GSE, which has the largest  $\beta$ ;

- Were the  $kn$ LS distribution a perfect Gaussian centered at  $\langle s^{(k)} \rangle = k$ , the  $kn$ SFF would only involve the Gaussian envelope and the cosine term

$f_t^{(k)} = e^{-k^2 t^2 / (4\alpha)} \cos(kt)$  with frequency  $\omega_k = k$ , since the Fourier transform of a Gaussian is another Gaussian. The non-zero mean is accounted for by including  $e^{i\langle s^{(k)} \rangle t}$ , whose real part is  $\cos(kt)$ . Thus the sine term in the  $kn$ SFF comes from the non-Gaussianity of the  $kn$ LS distribution. This is studied in more detail in App. F.

With the approximation (53), the final expression for  $S_t^{(k)}$  becomes

$$S_t^{(k)} \approx \frac{2(N-k)}{N^2} e^{-\frac{\omega_k^2 t^2}{4\alpha}} \left[ \cos(\omega_k t) + \frac{1}{12\alpha} \omega_k t \left( \frac{\omega_k^2 t^2}{2\alpha} - 3 \right) \sin(\omega_k t) \right],$$

as also given in the summary, Eq. (12). Figure 8 shows that our analytical approximation above reproduces well the numerical data for all three Gaussian ensembles.

Before turning to the complete SFF, we study some more properties of the  $k$ th neighbor SFF: the  $k$ th dip time  $t_d$  and depth of  $S_t^{(k)}$  as a function of  $k$ , and the scaling of the deepest  $k^*$  neighbor as a function of  $N$ .

## 2. Dip time and depth of the $k$ th neighbor SFF

We define the  $k$ th dip time [53] for each  $S_t^{(k)}$  as the time the function reaches its minimal value. It can be computed from the exact expression with  $f_t^{(k)}$  given by (47), or from the approximate one, Eq. (12). However it may not be possible to analytically determine the minimum of those functions. One possibility to overcome this is to look at (12), where for large enough  $k$  (and not too large  $t$ ), the main contribution comes from the cosine. We know that its minimum happens when its argument is equal to  $\pi$ , therefore

$$t_d(k) \approx \frac{\pi}{\omega_k} \stackrel{(54)}{\approx} \frac{\pi}{k}. \quad (56)$$

Note that this result suggests that the  $k$ th dip time does not depend on the ensemble  $\beta$ , but only on the neighbor degree  $k$ . For a more detailed analysis of this approximation, see Appendix H. From this estimate, we can also find the  $kn$ SFF depth as a function of  $k$ , by plugging (56) into (12), we find the behavior

$$S_{t_d}^{(k)} \sim -\frac{2(N-k)}{N^2} e^{-\frac{\pi^2}{2k(\beta k + \beta + 2)}}. \quad (57)$$

Figure 9 shows that the approximation (56) for the dip time agrees with the numerical simulation from the different Gaussian ensembles and for the XXZ model, provided that the spectrum is unfolded. Figure 10 (left) shows that (57) characterizes well the  $k$ th dip time obtained from numerical random matrices.

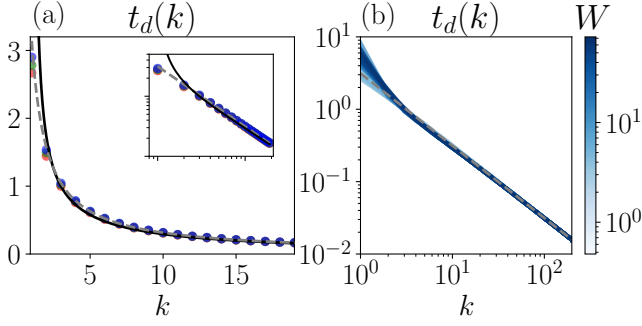


FIG. 9. **knSFF dip time** as a function of the neighbor degree for (a) ideal ensembles: Poisson (black), GOE (red), GUE (green) and GSE (blue) computed numerically from the unfolded spectrum along with the approximate expression (56) (dashed grey). **Inset:** same plot in log-log scale that shows explicitly the  $t_d(k) \sim k^{-1}$  dependence; and (b) for the XXZ spin chain for different values of the disorder (blue colorscale) along with the analytical result  $t_d(k) = \pi/k$  (dashed gray).

### 3. Scaling of the deepest $k$ -th neighbor SFF

The deepest  $k$ -th neighbor SFF, denoted by  $k^*$ , is computed from the minima of Eq. (57) for the Gaussian random matrix ensembles and (62) for the Poissonian ensemble (see next section). The physical significance of this value is the spectral distance  $k$  after which the  $k$ th dip of the  $kn$ SFF starts getting shallower. It is challenging to extract the minimum from the exact expression. If we take the large  $k$  approximation, we find the deepest  $k^*$  to be given approximately by the solutions of

$$k^{*2}(2 + \beta + \beta k^*) = N\pi^2, \quad (58)$$

whose exact solution can be found exactly using *Mathematica* but which is too cumbersome to understand. However, a large  $N$  expansion yields

$$k^* \sim \mathcal{C}_{\frac{1}{3}} N^{\frac{1}{3}} + \mathcal{C}_0 + \mathcal{C}_{-\frac{1}{3}} N^{-\frac{1}{3}} + \mathcal{O}(N^{-\frac{2}{3}}) \quad (59)$$

for the Gaussian ensembles, where the coefficients are given by  $\mathcal{C}_{\frac{1}{3}} = \left(\frac{\pi^2}{\beta}\right)^{\frac{1}{3}}$ ,  $\mathcal{C}_0 = -\frac{\beta+2}{3\beta}$ ,  $\mathcal{C}_{-\frac{1}{3}} = \frac{(2+\beta)^2 - 3\beta\pi^2}{9\beta^{\frac{2}{3}}\pi^{\frac{2}{3}}}$ .

Figure 10 (right) shows a good agreement between this expression and numerical random matrices for the three Gaussian ensembles.

To end this section, we recall that the total SFF is not self-averaging. We refer the reader to Appendix G which shows that the  $kn$ SFF for GUE (with similar conclusions for the other ensembles) is also not self-averaging.

### C. $k$ th neighbor SFF for the Poissonian ensemble

The averaged  $k$ th neighbor SFF can be computed for matrices with uncorrelated eigenenergies, in the same

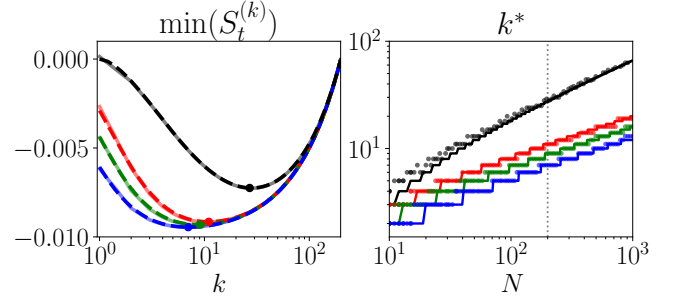


FIG. 10. (left) **Minimum value of  $kn$ SFF  $S_t^{(k)}$  as a function of the spectral distance  $k$ .** Approximate analytical results (dashed lines) for the RMT ensembles (57) and Poisson distribution (62), and numerical results (solid lines). Colors are as in Fig. 1, i.e. Poisson (black), GOE (red), GUE (green) and GSE (blue). The numerical results are obtained from matrices of dimension  $N = 200$  and averaged over  $N_{\text{av}} = 2000$  elements of the ensemble. (right) **Scaling of the deepest neighbor  $k^*$  as a function of the system size  $N$**  computed numerically for RMT and Poisson ensembles (circles) and the analytical approximations (59) and (64) rounded to the nearest integer (lines). Numerical results are averaged over  $N_{\text{av}} = 200$  matrices. We show a guide for the eye at  $N = 200$  (gray dotted line) which agree with the values of  $k^*$  used in Figure 12 for the Poissonian and GOE endpoints of  $W$ .

manner as for the Gaussian ensembles case, but now using the corresponding probability distribution, Eq. (7). We thus find

$$S_t^{(k)} = \frac{2(N-k)}{N^2} \frac{\cos(k \arctan t)}{(1+t^2)^{k/2}}. \quad (60)$$

The  $k$ th dip time, which we define to be the first minima of this function, can then be computed exactly as

$$t_d(k) = \tan\left(\frac{\pi}{1+k}\right). \quad (61)$$

Note that it diverges at  $k = 1$  because the first  $kn$ SFF for the Poissonian ensemble shows no dip and asymptotically goes as  $\pi/k$ , similarly to the Gaussian ensembles. The value of  $\langle S_t^{(k)} \rangle$  at the dip time is

$$S_{t_d}^{(k)} = \frac{2(N-k)}{N^2} \cos^k\left(\frac{\pi}{1+k}\right) \cos\left(\frac{k\pi}{k+1}\right). \quad (62)$$

This expression admits the asymptotic expansion

$$S_{t_d}^{(k)} = \frac{2(N-k)}{N^2} \left(-1 + \frac{\pi^2}{2k} - \frac{4\pi^2 + \pi^4}{8k^2} + \mathcal{O}(k^{-3})\right), \quad (63)$$

which leads to a third-order polynomial equation whose solution can be expanded for large  $N$ . We thus find the deepest  $kn$ SFF to scale as

$$k_0^* \sim \frac{\pi}{\sqrt{2}} N^{\frac{1}{2}} - \left(1 + \frac{\pi^2}{4}\right) + \mathcal{O}(N^{-\frac{1}{2}}), \quad (64)$$

which scales faster than for the Gaussian ensembles. Thus, the deepest  $kn$ SFF in the Poissonian ensemble happens for  $k^*$  larger than in the chaotic case, as seen in Fig. 10, which also shows good agreement of the above analytical approximation with the numerics.

#### D. Dynamical signatures of chaos ( $kn$ SFF) in the disordered XXZ

To test how the dynamical signatures of a real system match those of idealized models, we extract data for the  $kn$ SFF from the XXZ model with disorder. Figure 11 shows numerical results for the  $k$ th neighbor SFF for various values of  $k$ , where the behavior for a disorder strength of  $W = 1$  can be compared with  $W = 20$ . The plot shows how the numerical data deviate from Poisson and GOE. In particular the frequency of the oscillations is well captured by the analytical expressions, but the deviations from the analytical  $kn$ SFFs show up in the envelope, i.e. in the amplitude of the oscillations, which is narrower than GOE for  $W = 1$  and broader than Poisson for  $W = 20$ .

Figure 12 shows results for the minimum value of  $S_t^{(k)}$  as a function of  $k$  as well as the values of  $k^*$  as a function of the disorder strength  $W$ . The minimum of the  $kn$ SFF agrees very well with the Poisson and GOE limits because, as discussed previously, the most relevant corrections to the  $kn$ SFF are in the envelope, which for the first oscillation still does not have a big contribution. In particular,  $k^*$  exhibits a transition, similar to that probed by  $\langle r \rangle$ , as coded in the colorscale. The values of  $k^*$  at the two ends of the range of  $W$ , which correspond to integrable (large  $W$ ) and chaotic (small  $W$ ), are exactly those predicted from the Poissonian and GOE ensembles respectively, for the window size we used to extract the data (compare with Figure 10). The full SFF shown in Figure 26 follows the general behaviour of Poisson and GOE for large and small disorder respectively, even though Figure 2 shows more correlations than Poisson and less correlations than GOE at large  $k$ . The works [30, 31] consistently find no ‘correlation hole’ for large disorder in this model.

#### E. Summing it up: the complete SFF

We now add up the contributions from all spectral distances to write the total SFF and compare our approximate analytical results to numerical simulations. Using the approximations (12) for the  $k$ th neighbor SFF, the total averaged SFF for the Gaussian ensembles is given

approximately by:

$$S_t \approx \frac{1}{N} + \sum_{k=1}^{N-1} \frac{2(N-k)}{N^2} e^{-\frac{\omega_k^2 t^2}{4\alpha}} \left[ \cos(\omega_k t) + \frac{1}{12\alpha} \omega_k t \left( \frac{\omega_k^2 t^2}{2\alpha} - 3 \right) \sin(\omega_k t) \right]. \quad (65)$$

Figure 13 compares our analytical results with numerical results for the random matrix ensembles. It shows that for the Gaussian ensembles, the above approximate expression gives good results, even without using any exact results for  $S_t^{(k)}$ . In particular, the transition between the ramp and plateau is well captured for the three ensembles: smooth for GOE, ‘kink’ for GUE and ‘spike’ for GSE. The time at which this transition happens was first discussed in [15] and we provide an alternative rationale for it by decomposing the SFF into the contributions from odd and even spectral distances, see below. Importantly, all the ensembles, when unfolded, show the plateau time at  $t_p = 2\pi$ . This is consistent with the results in [15] which show the plateau for the Gaussian ensembles at  $t_p/(2\pi\bar{\rho}) = 1$ , in our case unfolding the spectra sets  $\bar{\rho} = 1$  and thus  $t_p = 2\pi$ . In Appendix J, we test the accuracy of the total result given in Eq. (65).

One question that naturally arises from the discussion below Eq. (54) is: how important is the contribution of the sines? Can we recover the full SFF from just summing over the cosine part? i.e. with a Gaussian approximation for the  $kn$ LS distribution. The answer is that we get a correlation hole, but no linear ramp, and that the sines contributions are especially important at the beginning of the ramp and at the transition to the plateau.

The total averaged SFF for the Poissonian ensemble is given exactly by

$$S_t^{(\text{Poisson})} = \frac{1}{N} + \sum_{k=1}^{N-1} \frac{2(N-k)}{N^2} \frac{\cos(k \arctan t)}{(1+t^2)^{k/2}}. \quad (66)$$

Although for  $k > 1$  the  $k$ th neighbor SFF for the Poissonian ensemble has a dip and shows some oscillations before flattening out (as can be seen in Figure 8), the full Poissonian SFF has no ‘dip’ or ‘correlation hole’, as expected for completely uncorrelated levels.

*Even and odd contributions.*— The approximation (12) for the ensemble average of the  $k$ th component of the Gaussian ensembles SFF is expressed as a combination of cosines and sines with frequency  $\omega_k$  given by (54). Figure 14 presents the numerical results for the even and odd level contributions, defined as

$$\langle \mathcal{S}_t^{(\text{even})} \rangle \equiv \frac{1}{2N} + \sum_{k \text{ even}} \langle \mathcal{S}_t^{(k)} \rangle \quad (67a)$$

$$\langle \mathcal{S}_t^{(\text{odd})} \rangle \equiv \frac{1}{2N} + \sum_{k \text{ odd}} \langle \mathcal{S}_t^{(k)} \rangle, \quad (67b)$$

for random matrices taken from GOE, GUE, and GSE ensembles of dimension  $N = 100$ . Inspecting the plots,

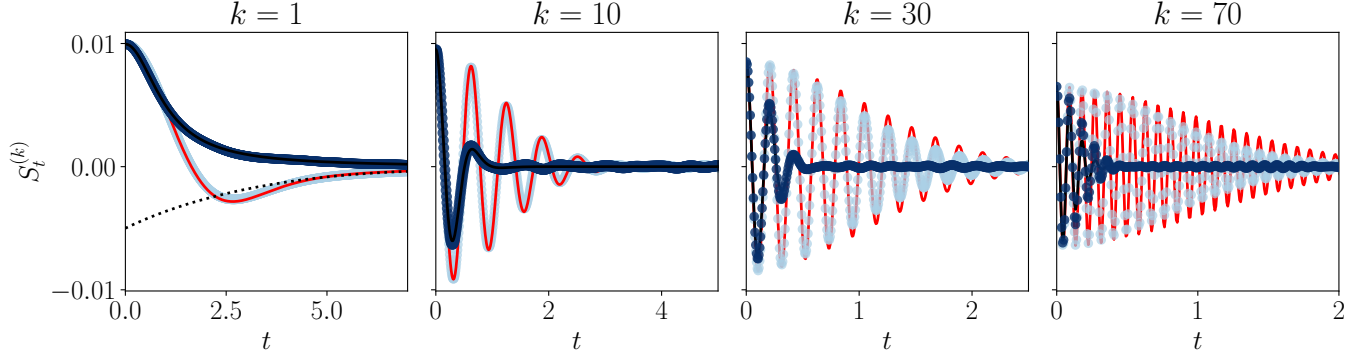


FIG. 11.  $k$ -th neighbor Spectral Form Factor for the disordered XXZ spin chain for different neighbor levels  $k = 1, 10, 30, 70$  in the chaotic ( $W = 1$ , light blue dots) and the integrable ( $W = 20$ , dark blue dots) phases along with the Poissonian (black line) and GOE (red line) curves. The deviation between the integrable phase and the Poissonian results is apparent starting from  $k = 10$ , and increases for larger  $k$ . Note that the oscillations differ only in their amplitude but not in their frequency. We emphasize the different scales in the time axis.

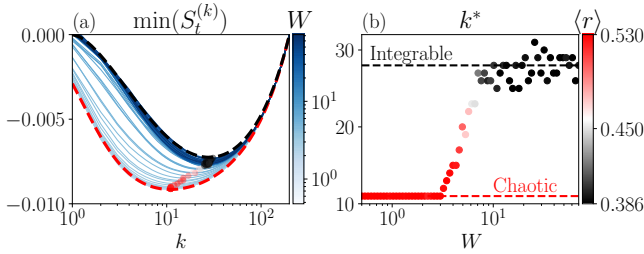


FIG. 12. (a) Minimum of the  $kn$ SFF as a function of the neighbor degree  $k$ , the colored dots mark the deepest  $kn$ SFF, (b) deepest  $k$ -th neighbors SFF  $k^*$  as a function of the disorder strength, the colorscale marks the  $\langle r \rangle$  parameter. The values of  $k^*$  for GOE and Poisson are  $k^* = 11$  and  $k^* = 28$  respectively, which can be obtained from the expansions for  $k^*$  (59), (64) respectively with  $N = 200$  which is the energy window size.

we find a constructive interference for  $\langle S_t^{(\text{even, odd})} \rangle$  at  $t \approx \pi$ . More specifically, there is a “resonance” for  $\langle S_t^{(\text{even})} \rangle$  and an “anti-resonance” for  $\langle S_t^{(\text{odd})} \rangle$  at  $t \approx \pi$ . This observation can be explained by our analytical results,

$$S_t^{(\text{even})} \approx \frac{1}{2N} + \sum_{k \text{ even}} C_N^{(k)} f_t^{(k)} \quad (68a)$$

$$S_t^{(\text{odd})} \approx \frac{1}{2N} + \sum_{k \text{ odd}} C_N^{(k)} f_t^{(k)}, \quad (68b)$$

where  $C_N^{(k)}$  is given by (38b) and  $f_t^{(k)}$  is given by the approximation (53). Taking  $\omega_k \approx k$ , the sum (68a) involves a sum of  $\cos(k t)$  with  $k = 2, 4, 6, \dots$  which interfere constructively at  $t = \pi$  to create a “peak” or a “resonance”; similarly, the sum (68b) involves a sum of  $\cos(k t)$  with  $k = 1, 3, 5, \dots$  which interfere constructively at  $t = \pi$  to create a “dip” or an “anti-resonance”. Interestingly, Fig. 14 also shows that most of the ramp is constructed from

the even neighbors. We also note that the ‘spike’ seen in the complete SFF for GSE (as can be seen in Fig. 13) is nothing but the next constructive interference from both the even and odd contributions, and happens (for the unfolded spectrum) at  $t = 2\pi$ . Note that the transition from the ramp to the plateau also happens at  $t_p = 2\pi$  for GUE and at a similar time for GOE.

Note that the fact that the GSE exhibits a spike is related to the Gaussian attenuation that multiplies the sum of cosines and sines in (65), which has the largest width of the Gaussian ensembles. Indeed, the width is set by  $\sqrt{\alpha}$ , which is proportional to  $\sqrt{\beta}$ , as per its definition in Eq. (5), and the GSE has the largest  $\beta$  (equal to 4). Fig. 15 shows the ratio of the plateau time  $t_p = 2\pi$  to the width of the Gaussian envelope for GOE, GUE and GSE. The envelope width is the largest for the GSE, in which the plateau time lies between 2 and 3 standard deviations of the Gaussian envelope.

*The partial SFF.*— In Eq. (15), we defined  $S_{t,K}$  which is the result of summing up  $S_t^{(k)}$  from  $k = 1$  to  $k = K$ . This helps us see how the total SFF is built up out of contributions from increasing values of  $k$ . In particular, as we add more and more  $S_t^{(k)}$  the minimum of the SFF moves to the left and gets deeper, as can be from the dip time in Fig. 16 (see App. C for further details on how the dip time is computed).

## F. The complete SFF with only nearest-neighbor correlations

As we have shown extensively in this article, the nearest-neighbor level spacing, although indicative of chaotic or regular behavior, is not a sufficient condition for chaos, since truly chaotic models (as modeled by RM) have correlations all over the spectrum. In this spirit, we construct a toy model which only has energy correlations to nearest neighbors, but nowhere else in the spectrum.

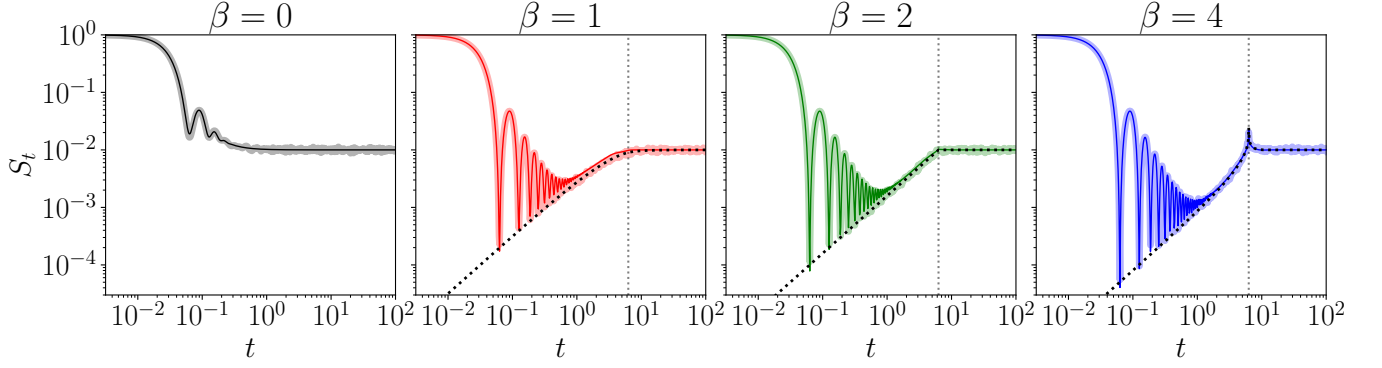


FIG. 13. **Spectral Form Factor** for: Poisson (black), GOE (red), GUE (green) and GSE (blue) computed numerically (thick transparent line) and using the analytical results (thin solid line) given by (66) (black) and (65) (red, green, blue). The connected SFF for each of the ensembles, see App. D, is also shown (black dotted line). The plots show results for random matrices with dimension  $N = 100$  and the numerics have been averaged over  $N_{\text{av}} = 1000$  matrices. The dotted gray line marks the start of the plateau at  $t_p = 2\pi$ .

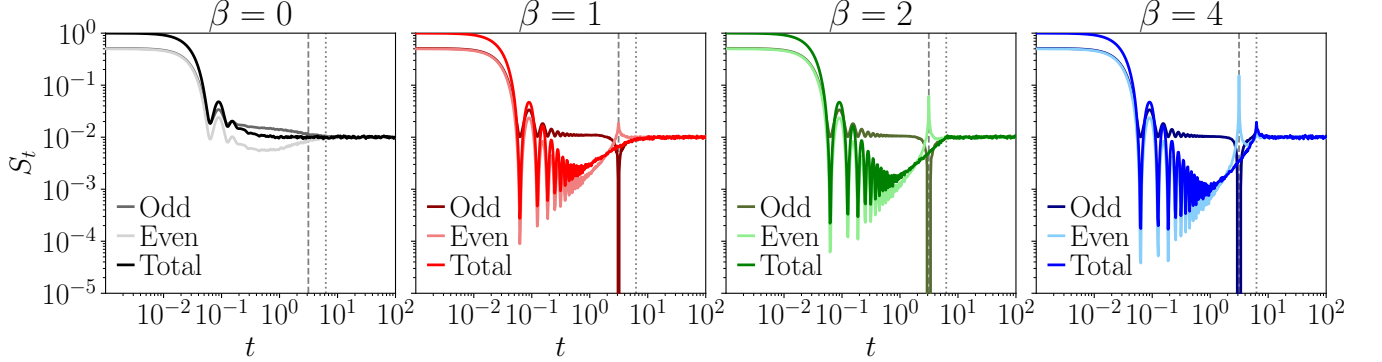


FIG. 14. **Odd vs even neighbor contributions to the SFF and their sum for Poisson, GOE, GUE and GSE**; computed numerically from  $N_{\text{av}} = 1000$  matrices of dimension  $N = 100$ . For visualization of the data in log-log scale, an extra factor of  $1/2N$  was added to the even and odd contributions. The even ones construct a ‘resonance’ while the odd ones construct an ‘anti-resonance’. The vertical lines highlight the time at which the resonance and anti-resonance happen,  $t^* = \pi$  (dashed gray), and at which the plateau starts for the Gaussian ensembles,  $t_p = 2\pi$  (dotted gray).

What would be the SFF of such a system? To answer this, let us recall that the probability distribution of the sum of two uncorrelated random variables  $z = x + y$  is given by their convolution. So, in this toy model, the second level spacing distribution simply reads

$$\begin{aligned} \mathcal{P}^{(2)}(s^{(2)}) &= \mathcal{P}^{(1)}(s^{(1)}) * \mathcal{P}^{(1)}(s^{(1)}) \\ &= \int_0^{s^{(2)}} ds \mathcal{P}^{(1)}(s) \mathcal{P}^{(1)}(s^{(2)} - s). \end{aligned} \quad (69)$$

The convolution theorem states that the Fourier transform of a convolution is the product of the Fourier transform, and vice versa. The  $kn$ SFF for this toy model follows as

$$S_t^{(k)} = \text{Re}(\mathcal{F}[\mathcal{P}^{(1)}]^k(t)), \quad (70)$$

where the Fourier transform of the nnLS distribution,

$\mathcal{F}[\mathcal{P}^{(1)}](t)$ , admits the exact expression

$$\begin{aligned} \mathcal{F}[\mathcal{P}^{(1)}](t) &= {}_1F_1\left(\frac{\beta+1}{2}, \frac{1}{2}, -\frac{t^2}{4A_\beta}\right) \\ &\quad - it {}_1F_1\left(\frac{\beta}{2} + 1, \frac{3}{2}, -\frac{t^2}{4A_\beta}\right). \end{aligned} \quad (71)$$

The sum of the  $kn$ SFF is shown in Fig. 17 for the GUE ensemble. The SFF of this toy model shows a correlation hole since it decays and grows back, but the ramp is not linear and therefore there is no chaos. Similar non-linear ramps in the SFF have been reported for integrable models like the SYK<sub>2</sub> [54, 55]. Thus, we conclude that correlations beyond the nearest energy levels are needed to find the linear ramp in the SFF characteristic of chaotic systems.

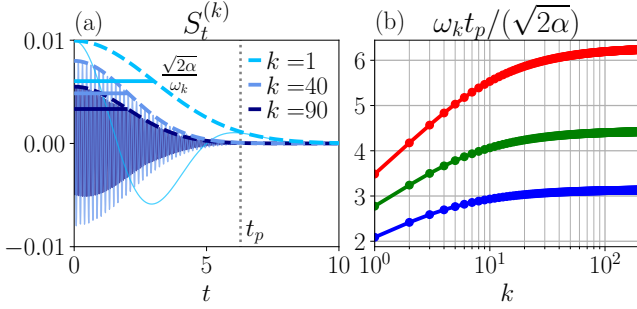


FIG. 15. (a)  $knSFF$  for GSE for  $k = 1, 40, 90$  (solid thin lines) and Gaussian envelope (dashed thick line), standard deviation of the Gaussian envelope  $\sqrt{2\alpha}/\omega_k$  (solid horizontal lines) and plateau time  $t_p = 2\pi$  (dotted gray line). (b) Ratio between the plateau time  $t_p = 2\pi$  and the width of the Gaussian envelope  $\sqrt{2\alpha}/\omega_k$  as a function of the neighbor degree  $k$  for the three Gaussian ensembles: GOE (red), GUE (green) and GSE (blue).

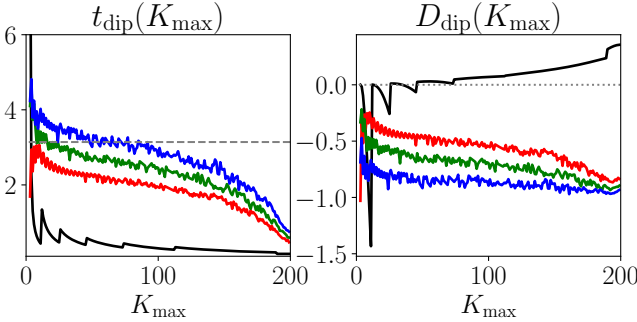


FIG. 16. **Dip time** (left) and **relative depth of the dip** (right) as a function of the maximum number of neighbors summed for the GOE (red), GUE (green) and GSE (blue). The plot also displays the "dip time" of Poisson (black), note that Poisson in general should have no dip, however some of its partial SFF's display a dip (see the plot in the right). When the relative depth is larger or equal to zero this time is associated with the plateau time. The results are computed from the analytical approximation of the SFF.

## V. A DISSIPATIVE PROTOCOL TO MEASURE THE $kNSFF$

The autocorrelation function of a general operator  $\hat{O}$  (39) can be obtained from knowledge of the spectrum and the operator. We propose a protocol, based on dissipative dynamics, to measure the  $k$ -neighbor autocorrelation function, introduced in (40).

Assuming that we are able to prepare an initial operator with non-zero weight only in its main and  $k$ -th diagonal, namely  $\hat{O}^{(k)} = \sum_{i=1}^N O_{ii} |i\rangle \langle i| + \sum_{i=1}^{N-k} O_{i+k,i} |i+k\rangle \langle i| + \text{h.c.}$ . Its autocorrelation function will be related to the  $knSFF$  since it only contains

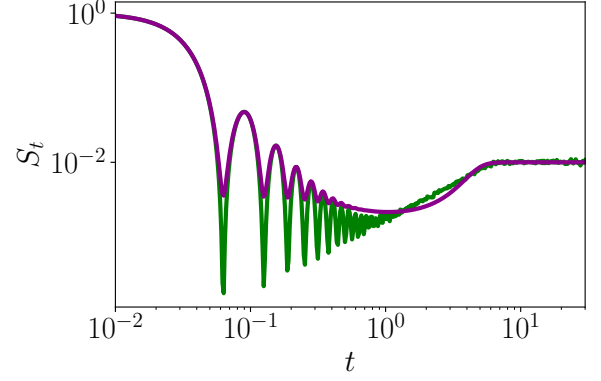


FIG. 17. SFF computed numerically for the GUE (green) and for the toy model with energy correlations to nearest neighbors only (purple), eq. (71).

spectral information from the  $knLS$ ,

$$\begin{aligned} C_t^{(k)} &= \frac{1}{\mathcal{N}^2} \text{Tr}(\hat{O}^{(k)} \hat{O}_t^{(k)}) \\ &= \sum_i \frac{|O_{ii}|^2}{\mathcal{N}^2} + \sum_{i=1}^{N-k} \frac{|O_{i+k,i}|^2}{\mathcal{N}^2} \cos[(E_{k+i} - E_i)t]. \end{aligned} \quad (72)$$

If at this point we further assume that we unfold the spectrum, so that the  $knLS$   $E_{i+k} - E_i$  does not depend on the density of states  $\rho(E_i)$ , and average over a suitable ensemble, we find that the time evolution (40) will depend on time only through  $f_t^{(k)}$ , which in turn completely determines the  $knSFF$ .

The initial operator  $\hat{O}^{(k)}$  might look somewhat artificial, so let us propose a way to engineer it through a dissipative evolution. In the case of dissipative dynamics in which the unitary part is dictated by  $\hat{H}_0$  and the dissipator consists of a single Hermitian jump operator  $\hat{L} = \hat{L}^\dagger$ , any system operator evolves according to the *adjoint Lindblad equation* [56, 57]

$$\partial_t \hat{O}_t = i[\hat{H}_0, \hat{O}_t] - \gamma[\hat{L}, [\hat{L}, \hat{O}_t]], \quad (73)$$

where  $\gamma$  is the dissipation rate associated with  $\hat{L}$ . Considering commuting operators,  $[\hat{H}_0, \hat{L}] = 0$ , which then share a common eigenbasis,  $\hat{H} = \sum_i E_i |i\rangle \langle i|$ ,  $\hat{L} = \sum_i l_i |i\rangle \langle i|$ , the solution of the above equation simply reads

$$\hat{O}_t = \sum_{i,j} O_{ij} e^{-i(E_i - E_j)t - \gamma(l_i - l_j)^2 t} |i\rangle \langle j|. \quad (74)$$

We now assume that we do not apply the Hamiltonian dynamics yet (e.g going to a rotating frame such that they are not relevant) and that we can engineer the jump operator in a way such that its eigenvalues repeat once after the  $k$ -th element, namely

$$\hat{L} = \text{diag}(l_1, \dots, l_k, l_1, \dots, l_k, l_{2k+2}, \dots, l_N), \quad (75)$$

where we have set  $l_{k+i} = l_i$  for  $1 \leq i \leq k$ , and we also consider no extra degeneracies  $l_i \neq l_j \forall i, j \in \{1, \dots, k, 2k+2, \dots, N\}$ . The evolution at a time  $T$  becomes  $\hat{O}_T = \sum_{i,j} O_{ij} e^{-\gamma(l_i - l_j)^2 T} |i\rangle \langle j|$ . All off-diagonal elements decay exponentially fast with time, except for those with  $|i - j| = k$  and  $i, j \in \{1, \dots, k\}$  which are preserved due to the structure of  $\hat{L}$ . Thus we see that  $\lim_{T \rightarrow \infty} \hat{O}_T = \hat{O}^{(k)} = \sum_{i=1}^N \hat{O}_{ii} |i\rangle \langle i| + \sum_{i=1}^{2k} O_{i+k,i} |i+k\rangle \langle i| + \text{h.c.}$ , i.e. this protocol leads to a matrix with  $2k$  nonzero elements only in the  $k$ -th diagonal. The full diagonal could be obtained by repeating the sequence of eigenvalues  $l_1, \dots, l_k$  more times in (75), but this would lead to higher “harmonics”, i.e. nonzero terms for  $|i - j| = 2k, 3k, \dots$ , which would contain contributions from higher degree  $kn$ SFFs.

Other possible experimental probes are to experimentally measure the energy levels of the system, and compute the  $kn$ LS distribution and the associated  $kn$ SFF by a Fourier transform. Alternatively, another way could be to use the formalism introduced in [58]. More specifically, one would need to find a partition the total Hilbert space in two,  $\mathcal{H} = \mathcal{H}_A \otimes \mathcal{H}_B$ , such that the condition  $\text{Tr}_B(\rho_B(E_i)\rho_B(E_j)) \propto \delta_{|i-j|,k}$  holds, where  $\rho_B(E_i) = \text{Tr}_A(|E_i\rangle \langle E_i|)$ . If there exists such a subspace  $\mathcal{H}_A$ , then the randomized measurement protocol devised in [58] could be readily used to compute the  $kn$ SFF’s and  $kn$ LS distribution.

## VI. SUMMARY AND DISCUSSION

In this work, we studied short, medium, and long-range spectral correlations and characterized their dynamical manifestation in the SFF. We found analytical results in random matrices taken from the three Gaussian ensembles (GOE, GUE, and GSE) and a model representative of integrable systems, i.e. an ensemble of completely uncorrelated energy levels (Poissonian ensemble) with uniform density of states. Real systems, as illustrated by the disordered XXZ spin chain, have spectral properties that lie in-between these ensembles.

Specifically, we focused on long-range spectral statistics in the form of the  $k$ th neighbor level spacing probability distribution and on the resulting  $k$ th neighbor spectral form factor. For the  $kn$ LS distributions, we introduced its variance as a probe that distinguishes chaos from integrability, with significantly different behaviors, and the Poissonian value  $k$  for the spacings  $s^{(k)}$  acting as an upper bound on the possible width of any  $\mathcal{P}^{(k)}(s)$  of a spectrum with correlated levels. We note here that the  $kn$ LS distributions can also be used to find the eigenvalue distribution of the Liouvillian superoperator, which consists of all energy differences, as we discuss in Appendix K. They also relate to the large  $N$  sine-kernel, see Appendix D.

Taking a Fourier transform of the  $kn$ LS distributions, we found expressions for the  $k$ th neighbor SFFs for the random matrix ensembles and for the Poissonian ensemble. By applying a few approximations, we could ex-

press the Gaussian ensemble  $kn$ SFF as a sum of cosines and sines with appropriate polynomial coefficients and an overall Gaussian envelope function. This realization of the  $kn$ SFF provides insight into the transition between the ramp and plateau for the different Gaussian ensembles. From studying the  $kn$ SFFs, we found that their minimum value as a function of  $k$  is markedly different between chaotic and integrable systems. In a similar spirit, we defined the  $k$ th neighbor decomposition of the autocorrelation function for operators.

For the Gaussian ensembles, the several approximations we made to achieve simple, tractable expressions capture the main properties of the complete SFF, as verified against numerical simulations. Our results show that the ramp feature found in the SFF of chaotic systems is a result of intricate relationships between  $kn$ SFFs of increasing spectral distances  $k$ . Specifically, the nearest-neighbor level repulsion only is not enough to induce a ramp. Also, the specific shape of the set of  $\mathcal{P}^{(k)}(s)$  and, in particular, the strong suppression at small  $s$  are important in achieving the specific features of the  $kn$ SFF which eventually build up the complete SFF. In particular, if the  $kn$ LS probability distributions were perfectly Gaussian, the results for the  $kn$ SFF would involve only a Gaussian envelope and a cosine term. Such a structure would not give rise to the specific features of the complete SFF, particularly around the transition from the ramp to the plateau. Hence, the non-Gaussianity of the  $kn$ LS distributions is crucial to capture the full chaotic signature of the SFF. We probe the non-Gaussianity of these distributions through the skewness and kurtosis in Appendix F. We further discuss the self-averaging properties of the individual  $kn$ SFFs in Appendix G.

This work opens many new directions for future study; we mention some below. We have made several approximations in our derivation of the  $k$ th neighbor level spacing distributions. While they capture the main behavior, we expect corrections at large  $k$ , and it would be interesting to study their effect on the  $kn$ SFFs and the full SFF in future work. Other possible directions include the study of how finite temperature affects the  $kn$ SFFs [59], or extending the  $kn$ LS and  $kn$ SFFs to the dissipative case, where mostly only nearest-neighbor correlations and SFF have been studied [60, 61]. We only began investigating how far the correlations between energy levels should persist in finding a linear ramp in the full SFF. We leave to future research the investigation of the  $k$ th neighbor autocorrelation functions we defined in this work. In particular, they can be used to understand better the behavior of the autocorrelation function for different operators. Lastly, one other possible extension of our results is in the field of *log-gases* [47]. In this context, the  $kn$ LS distribution  $\mathcal{P}^{(k)}(s)$  gives the strength of interaction between a particle and its  $k$ -th neighbor, resumming all the interactions with all the other particles.

To summarize, our results suggest that to investigate quantum chaos fully, it is important to include correlations at all spectral distances. Correlations beyond first

energy neighbors have a clear manifestation in dynamical quantities such as the spectral form factor, and will also show up in other time-dependent correlation functions. The specific nature of the level repulsion beyond just nearest-neighbor eigenenergies plays an important role in accurately capturing the complex features of many-body quantum systems at all time scales.

### ACKNOWLEDGMENTS

We would like to thank Lea F. Santos, Federico Balducci, András Grabarits, Aritra Kundu, Oskar Prosniaik, and Federico Roccati for insightful discussions and comments on the manuscript. Some of the numerical simulations presented in this work were carried out using the HPC facilities of the University of Luxembourg. This work was partially funded by the John Templeton Foundation (Grant 62171) and the Luxembourg National Research Fund (FNR, Attract grant 15382998). The opinions expressed in this publication are those of the authors and do not necessarily reflect the views of the John Templeton Foundation.

#### Appendix A: Numerical implementation of the Gaussian ensembles

In this appendix, we review the definitions and numerical construction of the three Gaussian random matrix ensembles: GOE, GUE, and GSE.

*GOE*: We sample a  $N \times N$  random matrix  $X$  with entries given from a real normal distribution with  $\sigma = 1$ , i.e.

$$X_{ij} = \mathcal{N}(0, 1), \quad 1 \leq i, j \leq N.$$

Matrices from GOE are symmetric, therefore  $H \in \text{GOE}(N)$  is given by

$$H = \frac{1}{2}(X + X^T).$$

*GUE*: Matrices from GUE are Hermitian, so their elements are generated from complex numbers, i.e.

$$X_{ij} = \mathcal{N}(0, 1) + i\mathcal{N}(0, 1), \quad 1 \leq i, j \leq N.$$

From  $X$ , we can generate a Hermitian matrix simply by

$$H = \frac{1}{2}(X + X^\dagger), \quad H \in \text{GUE}(N).$$

*GSE*: Generating matrices from the symplectic ensemble is slightly more involved. We need to generate a matrix  $X$  of dimension  $2N$

$$X_{ij} = \mathcal{N}(0, 1) + i\mathcal{N}(0, 1), \quad 1 \leq i, j \leq 2N,$$

and introduce the skew Hermitian matrix  $J$  defined as

$$J = \begin{pmatrix} 0 & -1 \\ 1 & 0 \end{pmatrix} \otimes \mathbb{1}_N.$$

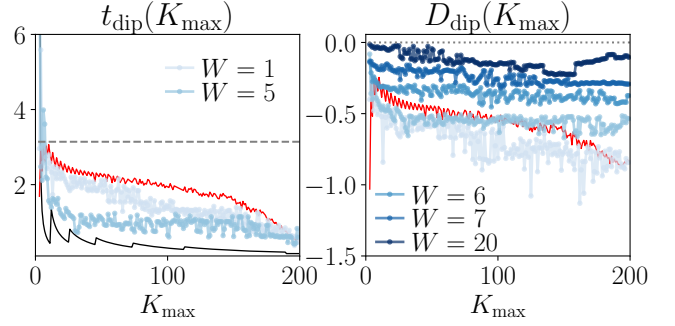


FIG. 18. Dip time (left) and relative depth of the dip (right) as a function of the maximum number of neighbors summed for XXZ model through the chaos to integrability transition.

Then, an element of the  $\text{GSE}(N)$  is given by

$$H = \frac{1}{2\sqrt{2}} (X + X^\dagger - J(X + X^\dagger)^T J).$$

#### Appendix B: Details of proof for $k$ th neighbor level spacing distribution

This appendix provides the explicit forms of  $\mathbf{A}$  and  $\mathbf{B}$  which appear in the quadratic polynomial  $\bar{q}(\{x_i\}_{i=1}^{k-1})$ .

The quadratic polynomial  $q(\{x_i\}_{i=1}^k)$  written in (21), once restricted by  $x_k = 1 - \sum_{i=1}^{k-1} x_i$ , takes the form

$$\begin{aligned} \bar{q}(\{x_i\}_{i=1}^{k-1}) &= \frac{k}{k+1} - 2 \sum_{i=1}^{k-1} \frac{k-i}{k+1} x_i \\ &+ \sum_{i=1}^{k-1} \frac{(k-i)(i+1)}{k+1} x_i^2 + 2 \sum_{i < j=1}^{k-1} \frac{(k-j)(i+1)}{k+1} x_i x_j. \end{aligned} \quad (\text{B1})$$

From here, we can read off the elements  $B_i$  and  $A_{ij}$  for  $i, j = 1, \dots, k-1$  as

$$B_i = \frac{k-i}{k+1}, \quad (\text{B2})$$

$$A_{ii} = \frac{(k-i)(i+1)}{k+1}, \quad (\text{B3})$$

$$A_{i \neq j} = \frac{(k - \max(i, j))(\min(i, j) + 1)}{k+1}. \quad (\text{B4})$$

It can be checked that  $\mathbf{A}$  is positive definite. The inverse of  $\mathbf{A}$  is a tridiagonal, almost Toeplitz matrix [62], with diagonal  $A_{11}^{-1} = 3/2$  and  $A_{ii}^{-1} = 2$  for  $i \neq 1$ , and off-diagonals  $A_{i,i+1}^{-1} = A_{i-1,i}^{-1} = -1$ . Also, it can be verified that  $\mathbf{m} = \mathbf{A}^{-1}\mathbf{B} = (1/2, 0, 0, \dots, 0)$ .

#### Appendix C: Computing the dip time of the SFF

The dip time is the time after which the SFF starts showing the linear ramp. Since the SFF in general has

non-universal behavior at short times, in particular for the unfiltered case it shows some oscillations which go under the dip, we cannot define the dip time just as the time at which the SFF has the deepest minimum. To overcome this problem in here we use the following algorithm :

1. Compute the array of relative maxima  $S_{t_{\text{MAX}}}$  and minima  $S_{t_{\text{MIN}}}$  of the SFF.
2. Compute the absolute minimum of the array of relative maxima, i.e. the maximum closest to the dip time  $t_{\text{MAX}}^{\text{D}} = \min_{t_{\text{MAX}}} S_{t_{\text{MAX}}}$ .
3. The dip time of the full SFF is then the closest minimum to the deepest maximum,  $t_{\text{dip}} = \min_{t_{\text{MIN}}} |t_{\text{MIN}} - t_{\text{MAX}}^{\text{D}}|$ .

Since in the ramp the SFF shows a lot of small oscillations because it is not self-averaging, these ensure that this algorithm will work correctly for as long as an actual dip exists. When the dip does not exist, e.g. in the integrable phase of the XXZ spin chain, the deepest maximum will be very affected by the quantum noise in the SFF signal. To capture the depth of the correlation hole we can define the relative depth as

$$D_{\text{dip}} = N \left( S_{t_{\text{dip}}} + \frac{1}{N} \right). \quad (\text{C1})$$

In Fig. 18 we show the dip time and relative depth of the correlation hole for the partial  $K_{\text{max}}$  neighbors SFF. The results for  $W = 1$  follow the general trend from GOE: i.e. summing the first few neighbors gives a larger contribution to the dip time while the further apart neighbors do not affect the dip time so much. As we get closer to the integrable zone most of the dip time is explained by the first few neighbors, with the further apart ones having much smaller contribution. We do not show the dip time in the integrable phase because it is completely governed by noise, but the depth suggests that the correlation hole closes.

#### Appendix D: The connected SFF for Gaussian ensembles and sine-kernel

The 2-point spectral connected correlation function  $\rho_c(E, E')$  of a certain ensemble is defined as [3]

$$\rho_c(E, E') = \langle \rho(E)\rho(E') \rangle - \langle \rho(E) \rangle \langle \rho(E') \rangle, \quad (\text{D1})$$

where  $\rho(E) = \sum_j \delta(E - E_j)$  and  $\langle \bullet \rangle$  represents a suitable average, e.g. over the random matrix ensemble. Thus  $\langle \rho(E) \rangle$  is the average density of states. After unfolding, i.e. introducing the rescaled energies  $\varepsilon = EN\langle \rho(E) \rangle$ , the renormalized 2-point correlation function reads

$$\frac{\rho_c(E, E')}{\langle \rho(E) \rangle \langle \rho(E') \rangle} = \delta(\varepsilon - \varepsilon') - Y(\varepsilon, \varepsilon'), \quad (\text{D2})$$

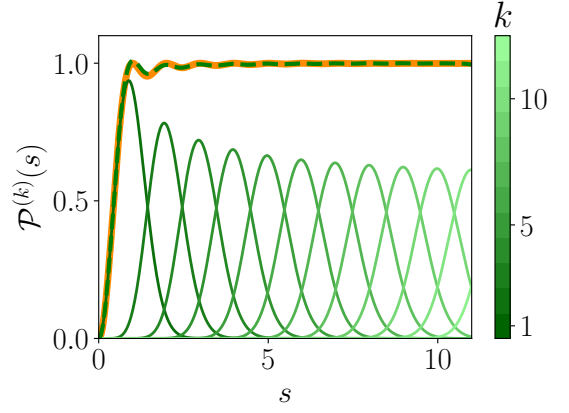


FIG. 19.  $\mathcal{P}^{(k)}(s)$  distribution for GUE for the first 12 neighbors (green lines), along with sine kernel  $1 - \text{sinc}^2(\pi s)$  (orange) and sum of the distributions (green dashed lines).

where  $Y(\varepsilon, \varepsilon')$  is *Dyson's two-level cluster function*, defined as

$$Y(\varepsilon, \varepsilon') = 1 - \left\langle \sum_{m \neq n} \delta(\varepsilon - \varepsilon_n) \delta(\varepsilon' - \varepsilon_m) \right\rangle. \quad (\text{D3})$$

This function depends only on the difference  $s = \varepsilon - \varepsilon'$  and for the GUE in the large  $N$  limit reads [3]

$$Y^{\text{GUE}}(s) = \text{sinc}^2(\pi s), \quad (\text{D4})$$

where the sinc function is defined as  $\text{sinc}(x) = \sin(x)/x$ . This is typically known in the literature as the sine-kernel. The 2-point correlation function is closely related to it through  $R_2(s) = 1 - Y_2(s)$ . Which can be obtained as a sum of the knLS level spacing distributions [43]

$$R_2(s) = \sum_{k=1}^{\infty} \mathcal{P}^{(k)}(s). \quad (\text{D5})$$

Figure 19 compares the sum of the  $knLS$  distributions with the two level correlation function, as obtained from the sine kernel  $1 - \text{sinc}^2(\pi s)$ , showing a very good agreement between the two.

The connected SFF is defined as the Fourier transform of the connected correlation function. For the random matrix ensembles it can be obtained from the cluster function, for GUE it reads [3]

$$b_{\text{GUE}}(t) = \begin{cases} \frac{t}{2\pi N} & \text{for } t \leq 2\pi \\ \frac{1}{N} & \text{for } t > 2\pi, \end{cases} \quad (\text{D6})$$

where we adapted it to our Heisenberg time of  $t_p = 2\pi$  and the plateau value of  $\lim_{t \rightarrow \infty} S_t = 1/N$ . For GOE it reads

$$b_{\text{GOE}}(t) = \begin{cases} \frac{t}{\pi N} - \frac{t}{2\pi N} \log\left(1 + \frac{t}{\pi}\right) & \text{for } t \leq 2\pi \\ \frac{2}{N} - \frac{t}{2\pi N} \log \frac{t+\pi}{t-\pi} & \text{for } t > 2\pi. \end{cases} \quad (\text{D7})$$

And lastly, for the GSE, it is

$$b_{\text{GSE}}(t) = \begin{cases} \frac{t}{4\pi N} - \frac{t}{8\pi N} \log(1 - \frac{|t|}{2\pi}) & \text{for } t \leq 4\pi \\ \frac{1}{N} & \text{for } t > 4\pi. \end{cases} \quad (\text{D8})$$

### Appendix E: Unfolding the spectrum

The spectrum of a system is a property which *a priori* depends on the system under consideration. However, its energy correlations can obey some universal laws. To study the latter, we need to remove the dependence of the spectrum on non-universal features, like the density of states  $\bar{\rho}(E)$ . In doing so, systems that are originally completely different can be compared. The procedure to remove the dependence on the local density of states is known as *unfolding* (see e.g. [63]). In this appendix, we explain how we unfold a generic spectrum. We then study some aspects of the effect of unfolding on our results.

Our method of unfolding involves computing the function

$$f(E) = N \int_{-\infty}^E dE' \bar{\rho}(E'). \quad (\text{E1})$$

where  $\bar{\rho}(E)$  is the average density of states, and then pass the energy eigenvalues  $\{E_i\}_{i=1}^N$  into this function to get the set of *unfolded* energy levels  $\{e_i\}_{i=1}^N = \{f(E_i)\}_{i=1}^N$ . For the random matrix ensembles we study, the average density of states is given by the Wigner semicircle distribution,  $\bar{\rho}(E) = \frac{1}{\pi\beta N} \sqrt{2N\beta - E^2}$ . This leads to an analytical form for the function  $f(E)$ , which reads [64]

$$f(E) = \frac{N}{2} + \frac{1}{\pi\beta} \left( N\beta \arcsin \frac{E}{\sqrt{2N\beta}} + \frac{E}{2} \sqrt{2N\beta - E^2} \right), \quad (\text{E2})$$

for  $-\sqrt{2\beta N} < E < \sqrt{2\beta N}$ , while it is  $f(E) = 0$  for  $E \leq -\sqrt{2\beta N}$  and  $f(E) = N$  for  $E \geq \sqrt{2\beta N}$ , see also [65].

For the disordered XXZ spin chain, there is no analytical expression for the average density of states. We thus rely on a *numerical* polynomial fit for  $f(E)$  for each realization of disorder. We used a larger window of energies to perform the fit, and then discarded the two edges, thus focusing our analysis on a window of around  $N = 200$  energies.

Our numerical unfolding depends on two parameters: the maximum order of the polynomial fit  $\eta$  and the number of bins with which we construct our histogram (related to the bin's width). These parameters, especially the polynomial order, can critically change the results since we can be overfitting the spectrum and include some of the universal correlations into the density of states. To check which minimum order gives a reasonable fit, we compare the numerical and analytical unfolding on a random matrix and define a *quality of the fit*,  $\mathcal{Q}$ , as the square of the difference between the histograms of the

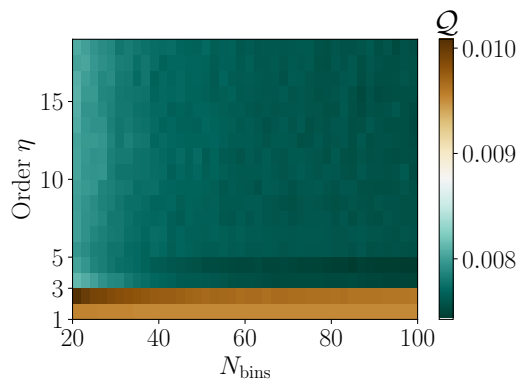


FIG. 20. Quality of the unfolding as a function of the order and the number of bins for the GOE.

analytical and numerical unfolded spectra, namely

$$\mathcal{Q} = \sum_{n \in \text{bins}} (\text{Hist}_n(f^{\text{ana}}(E)) - \text{Hist}_n(f^{\text{num}}(E)))^2. \quad (\text{E3})$$

Figure 20 shows that  $\eta = 3$  is an unfolding order with already good results. So, we chose this order to avoid over-fitting. The parameter of the number of bins is not too critical, and we set  $N_{\text{bins}} = 50$  to have enough bins and enough points per bin.

#### 1. Our results without unfolding

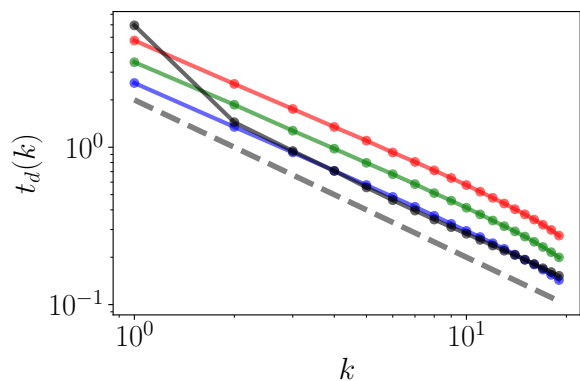


FIG. 21. Dip time as a function of the neighbor degree for Poisson (black), GOE (red), GUE (green) and GSE (blue) computed numerically from the folded spectrum along with an  $t_d(k) \sim k^{-1}$  dependence (dashed gray).

Although our results refer to the unfolded spectrum, we study here some of the same results for the folded (i.e. the original, *not* unfolded spectrum), namely, the dip times for the  $kn$ SFFs and the even-odd signatures discussed in Section IV E. We also compare the total folded vs unfolded SFF for disorder XXZ spin chain at two values of the disorder parameter  $W$  representative of the integrable and chaotic phases.

As can be seen in Figure 21, the dip times for the folded  $kn$ SFFs of the Gaussian ensembles no longer follow the relation  $t_d \approx \pi/k$  perfectly. However, they still follow a  $t_d(k) \sim k^{-1}$  decay with small corrections.

Another interesting aspect of unfolded versus folded results is whether the even-odd signatures, described in Section IV E, are still present without unfolding. Figure 22 confirms that such a signature is still present in Random Matrices and Fig. 23 shows how the anti-resonance dies out in the chaos to integrability transition for the XXZ spin chain without unfolding. The main difference is in the time at which the ‘resonance’ and ‘anti-resonance’ appear: while for the unfolded spectrum, they appear at  $t = \pi$ , for the folded spectrum, they appear at a time scale related to the matrix dimension.

The spectral distance decomposition of the SFF can also be applied to the SFF for the not unfolded XXZ spin chain, see Fig. 24. In this plot we see how in the chaotic phase adding more and more neighbors builds a longer and longer ramp. This still happens right before the transition, for  $W = 5$ , where we see a smaller correlation hole, which can be built from the first few neighbors. Figure 25 shows how adding more and more neighbors contributes to the dip time and the relative depth of the dip. Interestingly, for the chaotic phase the dip time follows a  $1/\sqrt{K_{\max}}$  power law.

For completeness, we compare the unfolded with the folded results for the total SFF of disordered XXZ spin-

chain at two values of  $W$ , see Figure 26.

### Appendix F: How good is a Gaussian approximation for the $kn$ LS distribution?

As discussed in the main text, the non-Gaussianity of the  $kn$ LS distributions is important for recovering the specific features of the total SFF. The non-Gaussianity of a distribution can be measured through quantities such as the skewness, characterizing the asymmetry of the distribution, and the kurtosis, characterizing the tailed-ness of the distribution. They are defined as

$$\text{Skew}^{(k)} = \mathbb{E} \left[ \left( \frac{s^{(k)} - \mu}{\sigma} \right)^3 \right], \quad (\text{F1})$$

$$\text{Kurt}^{(k)} = \mathbb{E} \left[ \left( \frac{s^{(k)} - \mu}{\sigma} \right)^4 \right], \quad (\text{F2})$$

where  $\mathbb{E}[\bullet] = \int_0^\infty \mathcal{P}(s) \bullet ds$  is the expectation value,  $\mu$  is the mean and  $\sigma$  is the standard deviation of the distribution. Note that these do not depend on whether or not we rescale the spacings by the average  $k$ . Using the generalized Wigner distribution,  $\mathcal{P}^{(k)}(s) = C_\alpha s^\alpha e^{-A_\alpha s^2}$  as in Eq. (4), we find

$$\text{Skew}_\beta^{(k)} = \frac{\sqrt{2} \left( 4\Gamma\left(\frac{\alpha}{2} + 1\right)^3 - (2\alpha + 1)\Gamma\left(\frac{\alpha}{2} + 1\right)\Gamma\left(\frac{\alpha+1}{2}\right)^2 \right)}{\left( (\alpha + 1)\Gamma\left(\frac{\alpha+1}{2}\right)^2 - 2\Gamma\left(\frac{\alpha}{2} + 1\right)^2 \right)^{3/2}}, \quad (\text{F3})$$

$$\text{Kurt}_\beta^{(k)} = \frac{-12\Gamma\left(\frac{\alpha}{2} + 1\right)^4 + (\alpha + 1)(\alpha + 3)\Gamma\left(\frac{\alpha+1}{2}\right)^4 + \pi 4^{1-\alpha}(\alpha - 1)\Gamma(\alpha + 1)^2}{\left( (\alpha + 1)\Gamma\left(\frac{\alpha+1}{2}\right)^2 - 2\Gamma\left(\frac{\alpha}{2} + 1\right)^2 \right)^2}. \quad (\text{F4})$$

In turn, the distribution from the Poissonian ensemble (7) yields

$$\text{Skew}_0^{(k)} = \frac{2}{\sqrt{k}}, \quad \text{and} \quad \text{Kurt}_0^{(k)} = 3 + \frac{6}{k}. \quad (\text{F5})$$

The expressions for the Gaussian ensembles admit the asymptotic expansions

$$\text{Skew}_\beta^{(k)} = \frac{1}{\sqrt{2\alpha}} + \mathcal{O}(\alpha^{-3/2}), \quad \text{Kurt}_\beta^{(k)} = 3 + \frac{3}{4\alpha^2} + \mathcal{O}(\alpha^{-3}), \quad (\text{F6})$$

which show that both the (excess) kurtosis and the skewness go to zero faster as a function of  $k$  in RMT than in Poisson. In other words, as we increase  $k$ , the generalized Wigner distribution approaches a Gaussian distribution faster than the Poisson results do. This result is expected in the literature for the distribution of  $kn$ LS [66]. Figure

27 shows the comparison with numerical random matrices. We see that a real random matrix has a skewness that follows the derived power-law for small  $k$ , but starts decaying faster until it changes sign at  $k = N/2$ , i.e. the distribution after this point becomes asymmetric with a tail to the right. Interestingly, the skewness for  $k \sim N$  looks opposite to the one for small  $k$ , which suggests that the function is antisymmetric around  $k = N/2$ . The kurtosis for random matrices, however, behaves very differently from the derived power laws, from which we conclude that the tails of the  $kn$ LS distribution are not well captured by the generalized Wigner surmise. Note that these results are considering the full extent of a random matrix, while the validity of our results is constrained to the center of the semicircle law.

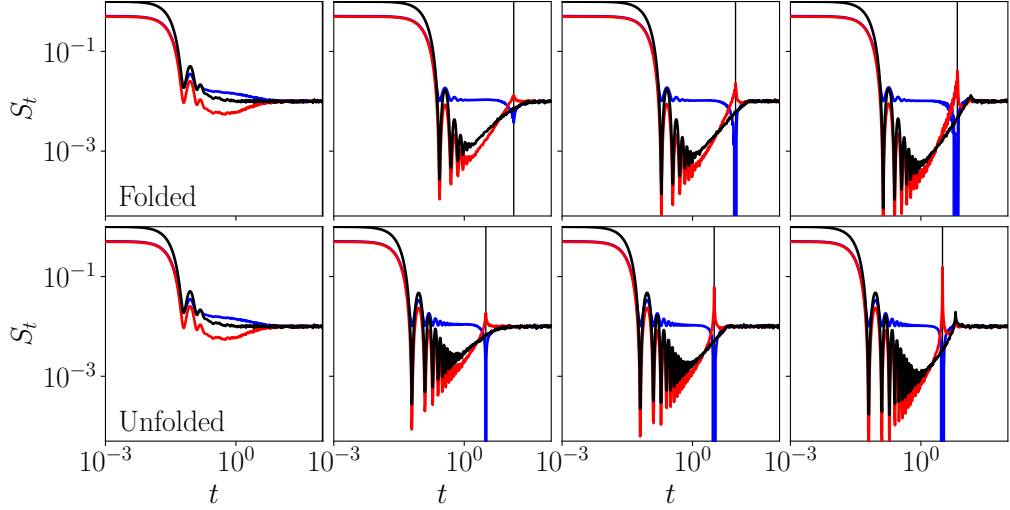


FIG. 22. The even- (red) and odd- (blue) neighbor contributions are compared for the folded and unfolded cases of Poisson, GOE, GUE, and GSE (left to right). The black solid line is the total SFF. The figure shows numerical data from random matrices of dimension  $N = 100$  averaged over  $N_{\text{av}} = 1000$  realizations.

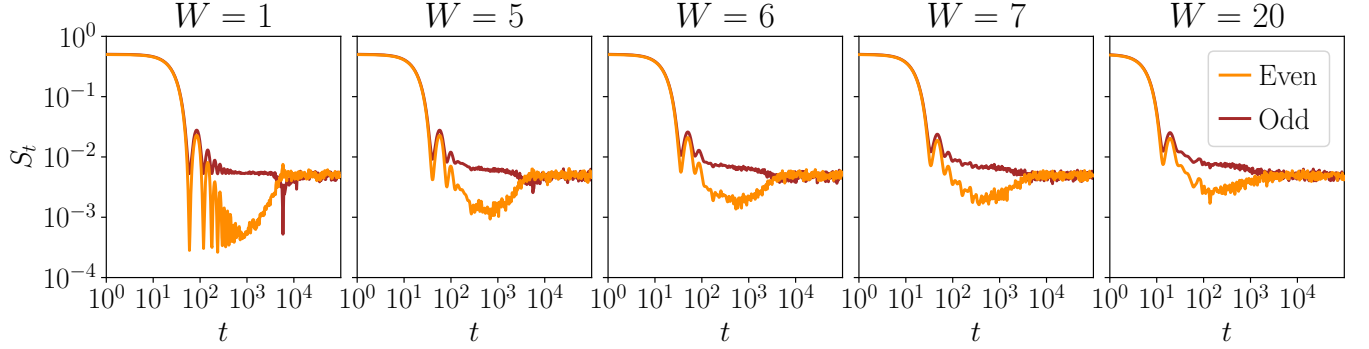


FIG. 23. Even (orange) and odd (brown) neighbor contributions to the SFF for the XXZ model without unfolding across the chaos (left) to integrability transition (right). Results are averaged over  $N_{\text{av}} = 50$  realizations of the onsite disorder.

### Appendix G: Self-averaging of the $k$ th neighbor SFF

In this appendix, we discuss the self-averaging properties of the  $k$ th neighbor SFFs, as a function of  $k$ .

A quantity is said to be self averaging if its relative variance becomes smaller as the system size is increased. The SFF is known to be particularly not self-averaging around its plateau (the flat part which the SFF tends to at large  $t$ ), i.e. the relative variance of its plateau increases as  $N$  is increased. Here, we numerically study the self-averaging of the plateau of the  $k$ th neighbor SFF. The relative variance of the  $k$ th neighbor SFF can be defined as (see e.g. [31]):

$$R_k(t) = \frac{\langle (\mathcal{S}_t^{(k)} + \bar{\mathcal{S}})^2 \rangle - \langle \mathcal{S}_t^{(k)} + \bar{\mathcal{S}} \rangle^2}{\langle \mathcal{S}_t^{(k)} + \bar{\mathcal{S}} \rangle^2}, \quad (\text{G1})$$

where  $\bar{\mathcal{S}} = \frac{1}{N(N-1)}$  is the value of the plateau divided equally among the  $N - 1$  possible neighbors, which we

added such that the average  $\langle \mathcal{S}_t^{(k)} + \bar{\mathcal{S}} \rangle$  is non-zero.

Figure 28 shows the relative variance of the plateau as a function of the neighbor degree  $k$  for different dimensions of the random matrices. We can observe several features:

- $\mathcal{S}_t^{(k)}$  is never self-averaging since the relative variance increases with the dimension of the matrix.
- The limiting value of the relative variance decreases linearly with  $k$  in the following way

$$\bar{R}_k^{\text{plat}} = \frac{1}{T} \int_{t_p}^{t_p+T} R_k(\tau) d\tau = (N - k) \frac{N - 1}{2N}, \quad (\text{G2})$$

where indeed Figure 28 suggests a linear function of  $k$  with a constant slope independent of  $N$  and a constant which scales linearly with  $N$ .

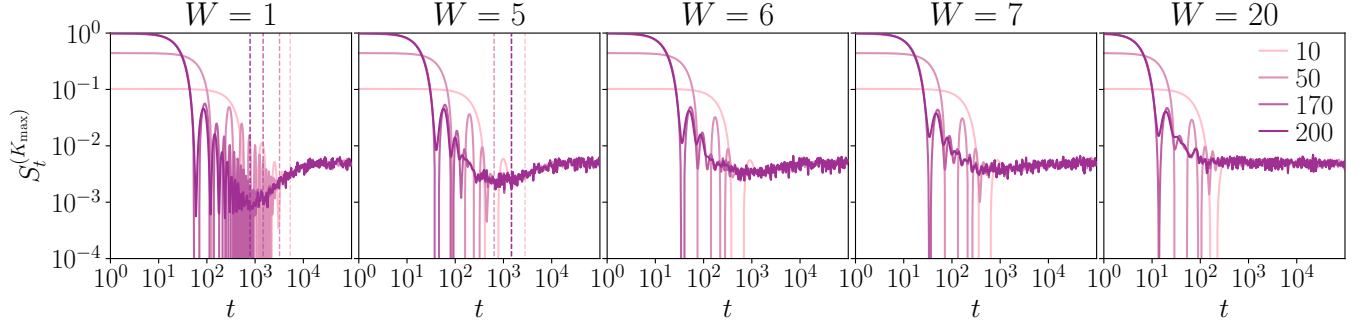


FIG. 24. **Spectral distance decomposition of the SFF for the XXZ spin chain** without unfolding the spectrum. The  $K_{\max}$  neighbors partial SFF is shown for  $K_{\max} = 10, 50, 170, 200$ . The results are averaged over  $N_{\text{av}} = 50$  realizations and the rest of the parameters are the same as Fig. 5

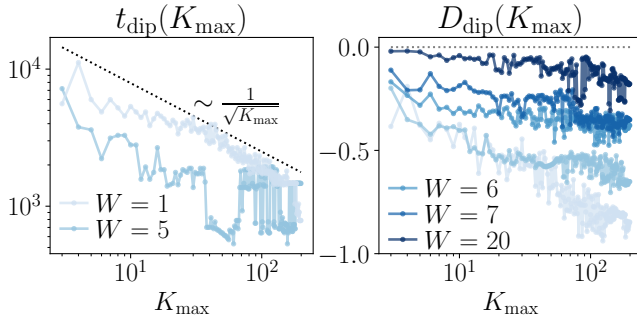


FIG. 25. Dip time (left) and relative depth (right) of the  $K_{\max}$  neighbors partial SFF for the XXZ model without unfolding the spectra. Scaling  $1/\sqrt{K_{\max}}$  (black dotted line, left) and mark for the eye at relative depth equal to zero (dotted gray, right). The parameters are the same as Fig. 24

#### Appendix H: Details on the $k$ -th dip time

To complete the discussion of the dip time in Section IV B, Fig. 29 compares the approximation (56) against the numerical dip times computed from the exact (47) and the approximate (12) analytical results. We see that (56) is a very good approximation of the dip time for  $k \geq 2$  and for  $k = 1$ , although there is a small dependence on  $\beta$  in the exact result, (56) is a better approximation than the dip time computed from (12). We therefore confirm our conclusion that the dip time of the  $kn$ SFF shows almost no dependence on the ensemble  $\beta$ .

#### Appendix I: The $k$ th neighbor autocorrelation functions

In this appendix, we complete some of the steps leading to the result (40) in Section IV A. Consider the infinite-temperature operator autocorrelation function for a Her-

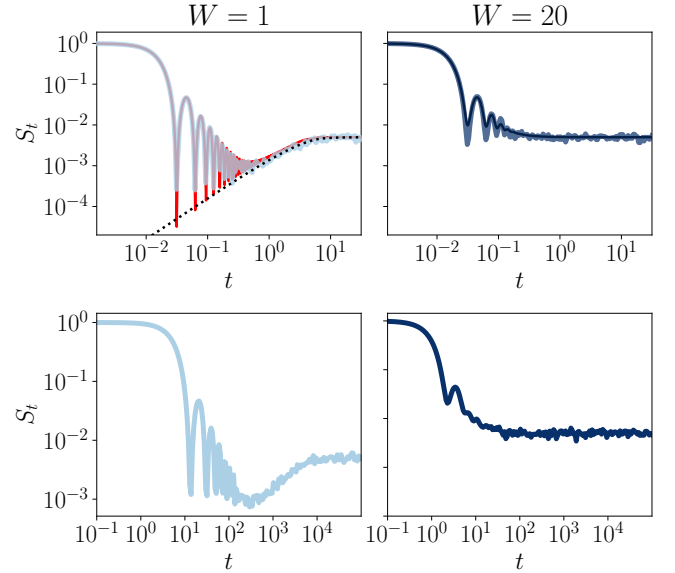


FIG. 26. **Spectral Form Factor** using the unfolded (up) or folded (down) spectrum of the XXZ spin chain with disorder strengths  $W = 1$  (left) and  $W = 20$  (right). The unfolded results (top) are compared with the RMT results (left, red dash-dotted) and the Poisson ensemble (right, black dash-dotted). The parameters are  $L = 16$ ,  $N_{\uparrow} = 8$ ,  $J_z = 2.21$ ,  $N_{\text{av}} = 100$ .

mitian operator  $O$  (i.e. an observable):

$$C_t \equiv \frac{\text{Tr}(O^\dagger O(t))}{\text{Tr}(O^\dagger O)} = \frac{1}{\mathcal{N}^2} \sum_{i,j=1}^N |O_{ij}|^2 \cos(E_i - E_j)t,$$

where  $O_{ij}$  are the matrix elements of the operator  $O$  in the energy basis and  $\mathcal{N}^2 = \sum_{i,j=1}^N |O_{ij}|^2$ . This expression can be decomposed according to level-spacing

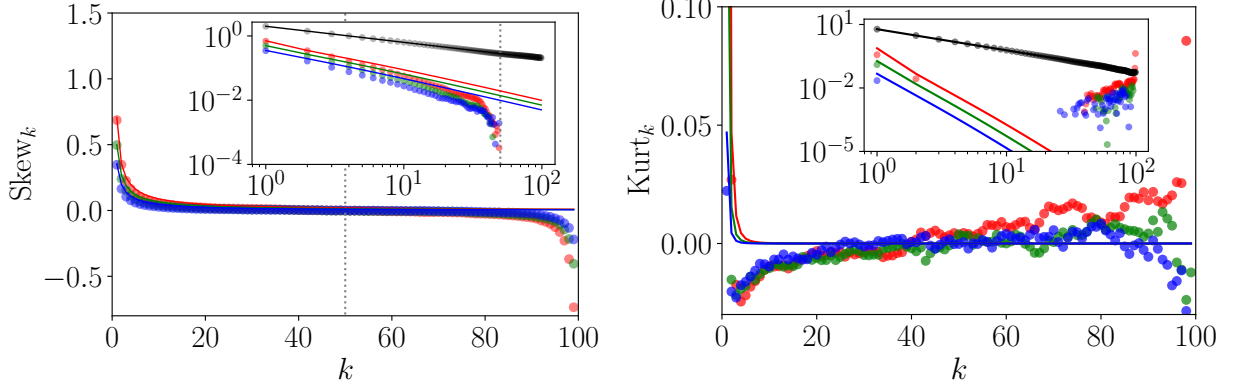


FIG. 27. Skewness and kurtosis for: GOE (red), GUE (green) and GSE (blue) computed from the asymptotic power laws (solid lines) and numerically (circles) for matrices of dimension  $N = 100$ . The numerical results use  $N_{\text{av}} = 10^5$  realizations of the ensemble. (insets) Skewness and Kurtosis in log-log scale, also show Poisson results (black). The value of  $k = N/2$  (dotted gray line).

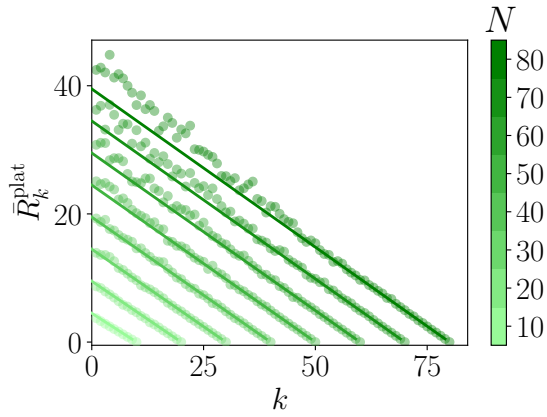


FIG. 28. Relative variance of the plateau of the  $kn$ SFF as a function of the neighbor degree  $k$ , for GUE random matrices of dimension  $N$  (colorscale). The results are averaged over  $N_{\text{av}} = 1000$  ensemble realizations and  $\bar{R}_k^{\text{plat}} := \frac{1}{T} \int_{t_p}^{t_p+T} R_k(\tau) d\tau$  is the time averaged relative variance on the plateau. Solid lines correspond to (G2).

distances, as follows

$$C_t = \frac{1}{\mathcal{N}^2} \sum_{i=1}^N |O_{ii}|^2 + \frac{2}{\mathcal{N}^2} \sum_{k=1}^{N-1} \sum_{i=1}^{N-k} |O_{i,i+k}|^2 \cos(ts_i^{(k)}). \quad (11)$$

Performing an ensemble average over the spectrum, which taken as unfolded ( $E_{i+k} - E_i$  does not depend on  $\rho(E_i)$ ) so that  $\mathcal{P}^{(k)}(s)$  can be used, the ensemble-averaged  $C_t$  can be re-written as

$$C_t = \frac{1}{\mathcal{N}^2} \sum_{i=1}^N |O_{ii}|^2 + \sum_{k=1}^{N-1} C_t^{(k)}, \quad (12)$$

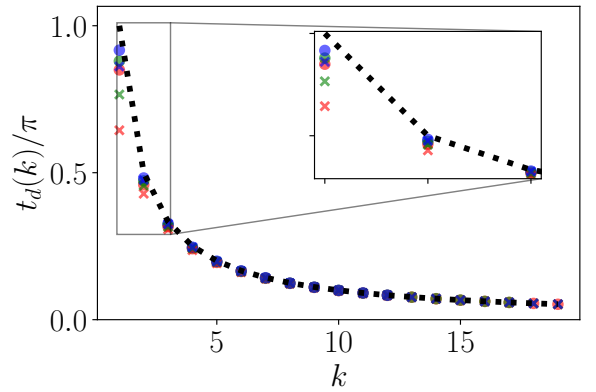


FIG. 29. Dip time as a function of neighbor-degree  $k$  for GOE (red), GUE (green) and GSE (blue) as computed numerically from exact expression (47) (circles), approximation of  $kn$ SFF (12) (crosses) and approximation of  $t_d(k)$  (56) (dotted line). The inset highlights the deviations for close neighbors in energy  $k = 1, 2, 3$ . The approximation (56) cancels some errors and gives a better estimate to the full analytics (47) than the values computed from (12)

where we defined the  $k$ th neighbor autocorrelation function

$$C_t^{(k)} \equiv O_N^{(k)} f_t^{(k)}, \quad (13)$$

with  $f_t^{(k)}$  defined in (38a) and with the coefficients

$$O_N^{(k)} \equiv \frac{2}{\mathcal{N}^2} \sum_{i=1}^{N-k} |O_{i,i+k}|^2. \quad (14)$$

## Appendix J: Test of the approximations for the SFF

Since we have made several approximations on the way to our final expressions for the total SFF for the Gaussian

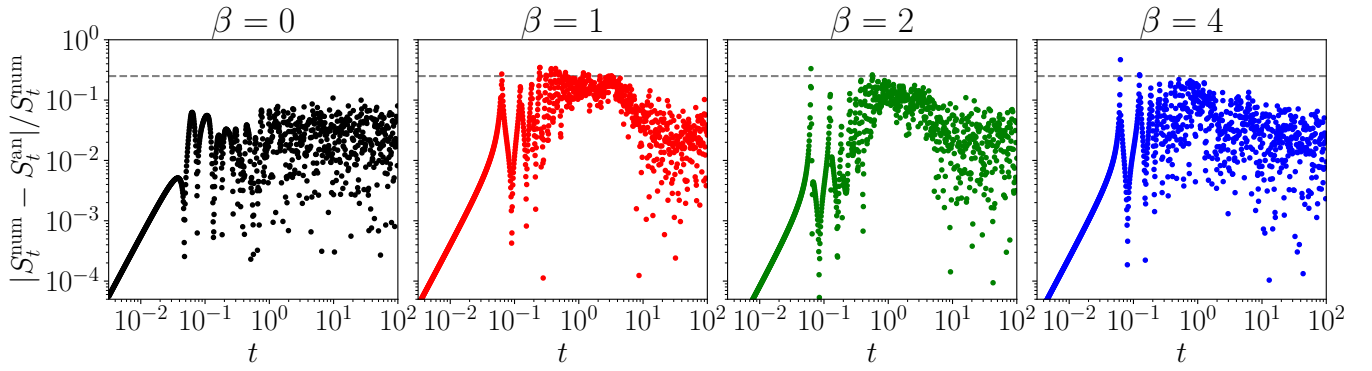


FIG. 30. **Difference between numerical and approximate analytical SFF** for: Poisson, GOE, GUE and GSE. The dashed line marks the 25% difference between the numerics and the analytics.

ensembles, (65), we test the validity of our approximate analytical expression. Figure 30 shows the relative error between the exact SFF (computed from numerical data) and the expression (65) for the three Gaussian ensembles, as well as a comparison between the Poissonian expression (66) and numerical data for the SFF taken from the Poissonian ensemble. We see that in GOE and GUE the approximation over-estimates slightly the ramp, and especially in GOE has a distance to it of around 25% of the value of the SFF at that point.

### Appendix K: Distribution of eigenvalues of the Liouvillian

The distributions  $\mathcal{P}^{(k)}(s)$  are closely related to the eigenvalue distribution of the Liouvillian, as we explain in this appendix.

In the case of unitary dynamics, the Liouvillian superoperator is defined as

$$\mathcal{L}(\bullet) \equiv [\hat{H}, \bullet], \quad (\text{K1})$$

in terms of the energies  $E_n$  and eigenvectors  $|n\rangle$  of  $\hat{H}$  the Liouvillian has the eigendecomposition  $\mathcal{L}(|n\rangle\langle m|) = (E_n - E_m) |n\rangle\langle m|$ , i.e. the eigenvalues of the Liouvillian are all the energy differences  $\lambda_{nm} = E_n - E_m$ . The probability density of  $\lambda_{nm}$  for  $n \neq m$  then is the sum of all the  $k$ nLS distributions [14]

$$\mathcal{P}(\lambda) = \frac{2}{N(N-1)} \sum_{k=1}^{N-1} (N-k) \mathcal{P}^{(k)}(\lambda). \quad (\text{K2})$$

This sum is shown in Fig. 31 where the RMT ensembles show the expected level repulsion around  $\lambda = 0$ , the Poisson ensemble shows initially a linear decay with  $\mathcal{P}_\beta(\lambda) \sim -\lambda$ . After the initial growth due to level repulsion GUE and GSE show oscillations, peaked at  $\lambda = k \in \mathbb{N}$ , with the oscillations being more pronounced in GSE.

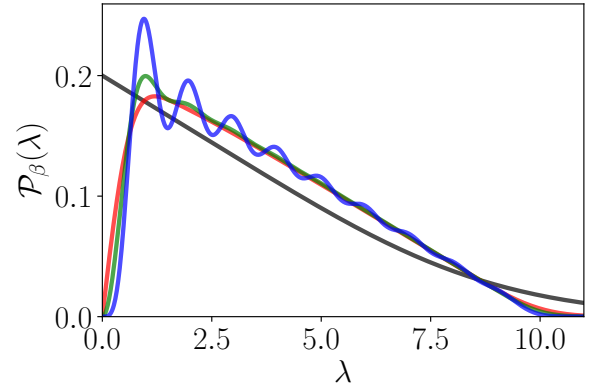


FIG. 31. **Distribution of eigenvalues of Liouvillian** computed from the analytical expressions with  $N = 10$  for: Poisson (black), GOE (red), GUE (green) and GSE (blue).

- 
- [1] J.-S. Caux and J. Mossel, Remarks on the notion of quantum integrability, *Journal of Statistical Mechanics: Theory and Experiment* **2011**, P02023 (2011).  
 [2] M. L. Mehta, *Random matrices* (Elsevier, 2004).  
 [3] F. Haake, *Quantum signatures of chaos* (Springer, 1991).  
 [4] E. P. Wigner, Results and theory of resonance absorp-

- tion, *Conference on Neutron Physics by Time of Flight* (1956), p. 59.  
 [5] E. P. Wigner, On the statistical distribution of the widths and spacings of nuclear resonance levels, *Mathematical Proceedings of the Cambridge Philosophical Society* **47**, 790–798 (1951).

- [6] M. Gaudin, Sur la loi limite de l'espacement des valeurs propres d'une matrice aléatoire, *Nuclear Physics* **25**, 447 (1961).
- [7] E. P. Wigner, Random matrices in physics, *SIAM Review* **9**, 1 (1967).
- [8] O. Bohigas, M. J. Giannoni, and C. Schmit, Characterization of Chaotic Quantum Spectra and Universality of Level Fluctuation Laws, *Physical Review Letters* **52**, 1 (1984).
- [9] M. V. Berry and M. Tabor, Level clustering in the regular spectrum, *Proceedings of the Royal Society of London. A. Mathematical and Physical Sciences* **356**, 375 (1977).
- [10] M. V. Berry, I. C. Percival, and N. O. Weiss, The bakerian lecture, 1987. quantum chaology, *Proceedings of the Royal Society of London. A. Mathematical and Physical Sciences* **413**, 183 (1987).
- [11] M. C. Gutzwiller, Periodic Orbits and Classical Quantization Conditions, *Journal of Mathematical Physics* **12**, 343 (2003), [https://pubs.aip.org/aip/jmp/article-pdf/12/3/343/10951718/343\\_1\\_online.pdf](https://pubs.aip.org/aip/jmp/article-pdf/12/3/343/10951718/343_1_online.pdf).
- [12] S. Wimberger, *Nonlinear dynamics and quantum chaos*, Vol. 10 (Springer, 2014).
- [13] L. Leviandier, M. Lombardi, R. Jost, and J. P. Pique, Fourier Transform: A Tool to Measure Statistical Level Properties in Very Complex Spectra, *Physical Review Letters* **56**, 2449 (1986).
- [14] J. Wilkie and P. Brumer, Time-dependent manifestations of quantum chaos, *Physical Review Letters* **67**, 1185 (1991).
- [15] Y. Alhassid and R. D. Levine, Spectral autocorrelation function in the statistical theory of energy levels, *Physical Review A* **46**, 4650 (1992).
- [16] J.-Z. Ma, Correlation Hole of Survival Probability and Level Statistics, *Journal of the Physical Society of Japan* **64**, 4059 (1995).
- [17] J. S. Cotler, G. Gur-Ari, M. Hanada, J. Polchinski, P. Saad, S. H. Shenker, D. Stanford, A. Streicher, and M. Tezuka, Black holes and random matrices, *Journal of High Energy Physics* **2017**, 118 (2017).
- [18] J. Cotler, N. Hunter-Jones, J. Liu, and B. Yoshida, Chaos, complexity, and random matrices, *Journal of High Energy Physics* **2017**, 48 (2017).
- [19] A. del Campo, J. Molina-Vilaplana, and J. Sonner, Scrambling the spectral form factor: Unitarity constraints and exact results, *Physical Review D* **95**, 126008 (2017).
- [20] A. Chenu, J. Molina-Vilaplana, and A. del Campo, Work Statistics, Loschmidt Echo and Information Scrambling in Chaotic Quantum Systems, *Quantum* **3**, 127 (2019).
- [21] A. Chenu, I. L. Egusquiza, J. Molina-Vilaplana, and A. del Campo, Quantum work statistics, Loschmidt echo and information scrambling, *Scientific Reports* **8**, 12634 (2018).
- [22] R. E. Prange, The Spectral Form Factor Is Not Self-Averaging, *Physical Review Letters* **78**, 2280 (1997).
- [23] M. Žnidarič, T. Prosen, and P. Prelovšek, Many-body localization in the heisenberg x x z magnet in a random field, *Physical Review B* **77**, 064426 (2008).
- [24] A. Pal and D. A. Huse, Many-body localization phase transition, *Physical Review B* **82**, 174411 (2010).
- [25] M. Serbyn and J. E. Moore, Spectral statistics across the many-body localization transition, *Physical Review B* **93**, 041424 (2016).
- [26] C. L. Bertrand and A. M. García-García, Anomalous thouless energy and critical statistics on the metallic side of the many-body localization transition, *Physical Review B* **94**, 144201 (2016).
- [27] P. Sierant and J. Zakrzewski, Level statistics across the many-body localization transition, *Physical Review B* **99**, 104205 (2019).
- [28] P. Sierant and J. Zakrzewski, Model of level statistics for disordered interacting quantum many-body systems, *Physical Review B* **101**, 104201 (2020).
- [29] J. Šuntajs, J. Bonča, T. Prosen, and L. Vidmar, Quantum chaos challenges many-body localization, *Physical Review E* **102**, 062144 (2020).
- [30] M. Schiulaz, E. J. Torres-Herrera, and L. F. Santos, Thouless and relaxation time scales in many-body quantum systems, *Physical Review B* **99**, 174313 (2019).
- [31] M. Schiulaz, E. J. Torres-Herrera, F. Pérez-Bernal, and L. F. Santos, Self-averaging in many-body quantum systems out of equilibrium: Chaotic systems, *Physical Review B* **101**, 174312 (2020).
- [32] H. Bethe, Zur theorie der metalle: I. eigenwerte und eigenfunktionen der linearen atomkette, *Zeitschrift für Physik* **71**, 205 (1931).
- [33] For  $\hat{T} = \hat{U}\hat{K}$  the anti-unitary time-reversal operator, generally written as the product of a unitary and complex-conjugation but which can be chosen as  $\hat{T} = \hat{K}$  [67], we verify that  $\hat{T}\hat{H}\hat{T}^{-1} = \hat{H}$  since the Hamiltonian is real.
- [34] W.-J. Rao, Higher-order level spacings in random matrix theory based on Wigner's conjecture, *Physical Review B* **102**, 054202 (2020).
- [35] D. Engel, J. Main, and G. Wunner, Higher-order energy level spacing distributions in the transition region between regularity and chaos, *Journal of Physics A: Mathematical and General* **31**, 6965 (1998).
- [36] A. Y. Abul-Magd and M. H. Simbel, Wigner surmise for high-order level spacing distributions of chaotic systems, *Physical Review E* **60**, 5371 (1999).
- [37] S. H. Tekur, U. T. Bhosale, and M. S. Santhanam, Higher-order spacing ratios in random matrix theory and complex quantum systems, *Physical Review B* **98**, 104305 (2018).
- [38] J. Sakhr and J. M. Nieminen, Wigner surmises and the two-dimensional homogeneous Poisson point process, *Physical Review E* **73**, 047202 (2006).
- [39] P. J. Forrester, A Random Matrix Decimation Procedure Relating  $\beta = 2/(r + 1)$  to  $\beta = 2(r + 1)$ , *Communications in Mathematical Physics* **285**, 653 (2009).
- [40] J. French, P. Mello, and A. Pandey, Statistical properties of many-particle spectra. ii. two-point correlations and fluctuations, *Annals of Physics* **113**, 277 (1978).
- [41] This result can be used to find a value for  $\alpha$  in (4), which would give us a correct value of the variance at large enough  $k$ . However, such an  $\alpha$  does not provide satisfying results for the full SFF when decomposed according to the  $kn$ SFFs, while the choice (5) does better at recovering the full SFF.
- [42] Where we are assuming no exact degeneracies in the spectrum.
- [43] A. Pandey, A. Kumar, and S. Puri, Quantum chaotic systems and random matrix theory (2019), published in: "21st Century Nanoscience: A Handbook (Ten-Volume Set)", edited by Klaus D. Sattler, CRC Press, [arXiv:1905.10596 \[cond-mat.stat-mech\]](https://arxiv.org/abs/1905.10596).
- [44] P. B. Kahn and C. E. Porter, Statistical fluctuations of

- energy levels: The unitary ensemble, *Nuclear Physics* **48**, 385 (1963).
- [45] M. V. Berry and P. Shukla, Geometric phase curvature for random states, *Journal of Physics A: Mathematical and Theoretical* **51**, 475101 (2018).
- [46] A. Y. Abul-Magd and M. H. Simbel, High-order level-spacing distributions for mixed systems, *Physical Review E* **62**, 4792 (2000).
- [47] P. J. Forrester, Log-Gases and Random Matrices (LMS-34), in *Log-Gases and Random Matrices (LMS-34)* (Princeton University Press, 2010).
- [48] F. J. Dyson, Statistical Theory of the Energy Levels of Complex Systems. I, *Journal of Mathematical Physics* **3**, 140 (1962).
- [49] We expect such a behavior for an unfolded spectrum ( $E_{i+k} - E_i$  does not depend on the local density of states  $\rho(E_i)$ ) which shows no mixed behavior, i.e. the spectral statistics does not change within the energy window.
- [50] S. Mirevski and L. Boyadjiev, On some fractional generalizations of the laguerre polynomials and the kummer function, *Computers & Mathematics with Applications* **59**, 1271 (2010).
- [51] See Digital Library of Mathematical Functions <https://dlmf.nist.gov/18.15#iv>.
- [52] Note that we are not expanding terms involving time in  $\alpha$ .
- [53] Note that we will use “ $k$ th dip time” for the minimum of the knSFF and “dip time” when referring to the full or partial SFF.
- [54] M. Winer, S.-K. Jian, and B. Swingle, An exponential ramp in the quadratic Sachdev-Ye-Kitaev model, *Physical Review Letters* **125**, 250602 (2020).
- [55] Y. Liao, A. Vikram, and V. Galitski, Many-body level statistics of single-particle quantum chaos, *Physical Review Letters* **125**, 250601 (2020).
- [56] H.-P. Breuer and F. Petruccione, *The theory of open quantum systems* (Oxford University Press on Demand, 2002).
- [57] A. Rivas and S. F. Huelga, *Open quantum systems*, Vol. 10 (Springer, 2012).
- [58] L. K. Joshi, A. Elben, A. Vikram, B. Vermersch, V. Galitski, and P. Zoller, Probing Many-Body Quantum Chaos with Quantum Simulators, *Physical Review X* **12**, 011018 (2022).
- [59] P. Martinez-Azcona and A. Chenu, Analyticity constraints bound the decay of the spectral form factor, *Quantum* **6**, 852 (2022).
- [60] L. Sá, P. Ribeiro, and T. Prosen, Complex Spacing Ratios: A Signature of Dissipative Quantum Chaos, *Physical Review X* **10**, 021019 (2020).
- [61] Z. Xu, L. P. García-Pintos, A. Chenu, and A. del Campo, Extreme Decoherence and Quantum Chaos, *Physical Review Letters* **122**, 014103 (2019).
- [62] Further properties of Toeplitz matrices can be found in <https://mathworld.wolfram.com/ToeplitzMatrix.html>.
- [63] T. Guhr, A. Muller-Groeling, and H. A. Weidenmuller, Random matrix theories in quantum physics: Common concepts, *Phys. Rept.* **299**, 189 (1998).
- [64] This result can be found in [https://robertsweeneyblanco.github.io/Computational\\_Random\\_Matrix\\_Theory/Eigenvalues/Wigner\\_Surmise.html](https://robertsweeneyblanco.github.io/Computational_Random_Matrix_Theory/Eigenvalues/Wigner_Surmise.html).
- [65] A. A. Abul-Magd and A. Y. Abul-Magd, Unfolding of the spectrum for chaotic and mixed systems, *Physica A: Statistical Mechanics and its Applications* **396**, 185 (2014).
- [66] T. A. Brody, J. Flores, J. B. French, P. Mello, A. Pandey, and S. S. Wong, Random-matrix physics: spectrum and strength fluctuations, *Reviews of Modern Physics* **53**, 385 (1981).
- [67] K. Kawabata, A. Kulkarni, J. Li, T. Numasawa, and S. Ryu, Symmetry of open quantum systems: Classification of dissipative quantum chaos, *PRX Quantum* **4**, 030328 (2023).